

# Prediction of curtain grouting efficiency based on ANFIS

Xiaochao Li<sup>1</sup> · Denghua Zhong<sup>1</sup> · Bingyu Ren<sup>1</sup> · Guichao Fan<sup>1</sup> · Bo Cui<sup>1</sup>

Received: 31 October 2016 / Accepted: 21 March 2017 / Published online: 31 March 2017  
© Springer-Verlag Berlin Heidelberg 2017

**Abstract** As an important method for improving dam foundations, curtain grouting is designed to create a hydraulic barrier to decrease permeability, enhance strength, and reduce deformability of rock masses. To evaluate the improvement of rock masses, the Lugeon value (LU), rock quality designation (RQD), and fracture filled rate (FFR) after grouting are key evaluation indicators of grouting efficiency. A prediction method based on an adaptive neuro-fuzzy inference system is proposed to predict and evaluate curtain grouting efficiency in this study. Geological factors (fracture intensity, LU, and RQD before grouting), effective grouting operation factors (effective grouting pressure, effective grouting time, effective grout volume, and effective cement take), and tested interval depth are considered to be the critical factors that greatly influence the efficiency of curtain grouting and are selected as input parameters for prediction models. The grouting efficiency evaluation indicators (the LU value, RQD, and FFR after grouting) are selected as output parameters for evaluation of the efficiency. In addition, a

formula for estimating the influence radius of grouting boreholes, which is used to determine the sphere of grouting influence, is proposed. To better reflect the influence of the position of grouting boreholes on the effects of grouting, this study suggests that the effective grouting operation factors can be calculated using an improved inverse distance weighting method. As a case study, this approach is used to predict the results of grouting and to evaluate the efficiency of curtain grouting in hydropower project A, located in the southwestern part of China. The approach shows considerable accuracy in predicting the results of grouting and evaluating grouting efficiency.

**Keywords** Curtain grouting efficiency prediction · Adaptive neuro-fuzzy inference system (ANFIS) · Grouting influence radius · Effective grouting operation factors · Improved inverse distance weighting (IDW) method · Ordinary Kriging (OK) method

---

✉ Denghua Zhong  
dzhong@tju.edu.cn

Xiaochao Li  
tju\_lixiaochao@tju.edu.cn

Bingyu Ren  
renby@tju.edu.cn

Guichao Fan  
fgc@tju.edu.cn

Bo Cui  
cuib@tju.edu.cn

<sup>1</sup> State Key Laboratory of Hydraulic Engineering Simulation and Safety, Tianjin University, 92 Weijin Road, Nankai District, Tianjin 300072, China

## Introduction

With the development of hydraulic engineering in China, many dams have been constructed in southwestern China during the past two decades. An important issue for such large-scale projects is the geological complexity of foundation rock masses, especially at sites involving faults and fractured zones, as well as weak interlayers between bedding structures (Chen et al. 2015; Lin et al. 2016). The quality of the foundation is fundamental to guaranteeing a dam's safety and reliability.

As an important method for reinforcing dam foundations, curtain grouting is used to inject grout material into the joints and cracks or voids of rock and soil formations so

that the engineering properties of these materials are improved through the decreased permeability, enhanced strength, and reduced deformability of the rock and soil formations (Yan 2014). There have been numerous examples of the successful application of curtain grouting to improve dam foundations. Successful dam curtain grouting has been proven effective in minimizing seepage and reducing permeability (Bryson et al. 2014; Sadeghiyeh et al. 2013; Uromeihy and Barzegari 2007), and the internal adhesive strength of the grouting material is also found to be important for strengthening when cementitious grout is used (Lin et al. 2016; Yang and Li 2008; Zolfaghari et al. 2015).

A common problem is how to verify the improvement. To evaluate grouting efficiency in the improvement of rock masses, some in situ tests such as water pressure tests (WPTs) (Ewert 1994), drilling and coring, borehole television imaging, acoustic velocity tests (Chen et al. 2015; Yang and Li 2008), and some geotechnical and geophysical tests (Kikuchi et al. 1997; Kim and Yoon 2014; Lynch et al. 2012; Utsuki and Mito 2014) have been commonly applied (Huang et al. 2012). Zolfaghari et al. (2015) developed a Q-logging system based on drilled cores to assess improvements in the rock mass mechanical properties through the  $Q$  parameters (e.g., RQD,  $J_n$ ,  $J_a$ ,  $J_r$  and  $J_w$ ) after grouting treatment was performed. Fan et al. (2016) proposed a comprehensive evaluation of curtain grouting efficiency based on the results of WPTs, drilling and coring, and borehole television imaging, including permeability (Lugeon value), rock quality designation (RQD), and fracture filled rate (FFR).

These in situ tests have been commonly used and may be the most direct and reliable ways to evaluate the grouting performance. In practice, however, because they are ex post evaluations, the efficiency of particular grouting operations is evaluated only when all these in situ tests are completed. In addition, the in situ tests have other shortcomings: (1) they are very time-consuming and expensive. To determine the quality of the grouting, many verification holes must be drilled, and tests such as WPTs must be performed, requiring considerable time and effort. (2) Because of the need to drill holes, improper handling will damage the integrity of the rock mass and result in leakage channels. (3) The locations of verification holes are mainly determined by experience and are easily affected by human factors. (4) As field sampling tests, the detection procedures cannot reflect the grouting quality of the entire section because of the nature of point measurements and the limitations of in situ point tests. Zadhesh et al. (2015) suggested that using predictive methods to assess the effects of grouting can be of great help in solving these problems.

However, since the dam foundation is below the surface of the ground, it is difficult to predict the results of grouting given the complexity of geological conditions and engineering operations. Numerous factors affect grouting efficiency. In discussions about the relationship between sealing efficiency and the factors that influence it, many researchers have described the mechanisms of grouting and sealing in a fractured rock mass, both practically and theoretically (Amadei and Savage 2001; Funehag and Fransson 2006; Gustafson and Stille 1996; Hässler et al. 1992a; Mortazavi and Maadikhah 2016; Saeidi et al. 2013; Shuttle et al. 2000; Yang et al. 2002). However, because of the complexity of geological conditions and engineering operations, a clearly specified relationship between sealing efficiency and the factors that influence it is still lacking (Sui et al. 2015). It is difficult to predict the results of grouting using theoretical analysis in practical engineering.

New artificial intelligence (AI) techniques, such as artificial neural networks (ANNs), fuzzy logic (FL), genetic algorithms (GAs), support vector machines (SVMs), and adaptive neuro-fuzzy inference systems (ANFISs), have been applied successfully to almost every problem in geotechnical engineering for many years (Jaksa et al. 2008; Shahin et al. 2001; Zadhesh et al. 2015). AI methods use data alone to determine the structure and parameters of the model and are well suited to modeling complex problems where the relationship between the model variables is unknown (Shahin et al. 2001). Within the field of grouting, ANN was introduced for the first time by Zettler et al. (1997). Since then, AI methods have been used in predicting cement take, groutability, etc. Li et al. (2001), Wang and Hao (2001), Yang (2004), and Zhang et al. (2007) applied ANNs to predict the cement take needed for grouting. Guo and Meng (2011) established a dynamic SVM model for cement take prediction. Liao et al. (2011), Hassanlourad et al. (2014) and Tekin and Akbas (2011) developed ANN-based models for the estimation of the groutability of granular soils. Tran and Hoang (2014) and Cheng and Hoang (2014) proposed SVM-based models for groutability prediction of permeation grouting projects. For the prediction of grouting efficiency, researchers have made several explorations and achieved some important results. Tinoco et al. (2011, 2012, 2014a, b) used SVM to predict the uniaxial compressive strength and the Young's modulus of columns produced by jet grouting. Lei et al. (2013) used SVM-based methods for regression to analyze test data and predict the strength of grouting concretion stone for the grouting of gravelly soil. Ehsanzadeh and Ahangari (2014) used ANFIS to predict the soilcrete column diameter produced by high-pressure jet grouting. To assess consolidation grouting quality, permeability in secondary boreholes was predicted by ANN by Zadhesh et al. (2015).

However, only a few studies have applied AI to engineering projects involving the grouting of rock masses by means of curtain grouting, and these studies were mainly confined to the prediction of cement take or grout volume. Research on predicting the efficiency of curtain grouting based on AI is rarely reported. In addition, previous studies used AI just as a single indicator prediction model for predictions in grouting. Permeability and the improvement in watertightness of rock masses are both very important in determining the efficiency of curtain grouting. Therefore, the permeability (LU value) and factors influencing the watertightness of rock masses, such as the RQD and FFR after grouting, should be taken into consideration to establish multiple prediction models to indicate curtain grouting efficiency.

The main objective of this paper is to present prediction models for evaluating the efficiency of curtain grouting using AI methods. In this article, an adaptive neuro-fuzzy inference system (ANFIS), which is a hybrid modeling method combining fuzzy logic and neural networks, is used to estimate the efficiency of curtain grouting. Based on the cited literature and engineering practice, geological and effective grouting operation factors, as well as the depth of the tested interval, are considered to be critical factors that can greatly influence the efficiency of curtain grouting in this paper. They are, therefore, selected as input parameters for the prediction models. The output parameters are comprehensive indicators of curtain grouting efficiency, including the LU value, RQD, and FFR after grouting. In this paper, a formula for estimating the influence radius of grouting boreholes is proposed. This paper uses the ordinary Kriging (OK) method to calculate the values of geological factors. To reflect better the influence of grouting borehole positions on the effects of grouting, this study proposes new parameters of effective grouting operation calculated by an improved inverse distance weighting (IDW) method. The models predict curtain grouting efficiency evaluation indicators and map the relationship between effectiveness indicators and influence factors, which is acquired by applying ANFIS to the training data. The improvement in the properties of dam foundations after grouting can be predicted accurately and quickly by using the prediction models. In addition, a case study is examined to confirm the validity and practicality of the proposed method.

The remaining parts of this paper are organized as follows: first, the research framework of this paper is introduced. Then, the methods for evaluating curtain grouting efficiency and obtaining the evaluation indicators, as well as determining the factors affecting grouting results, are explained. The methods used in this paper, including a formula for estimating the influence radius of grouting boreholes, an improved IDW method, the OK method and the ANFIS method, are presented in the next

section. Additionally, the paper provides a summary of the steps involved in using ANFIS-based prediction models to predict and evaluate the efficiency of curtain grouting. Then, the prediction model is applied to a dam curtain grouting project to show the effectiveness of the method, followed by discussion of the result. The conclusions of the study are listed in the final section.

## Research framework

As shown in Fig. 1, the research framework of this paper includes three major parts: obtaining the evaluation indicators and determining the influencing factors, establishing the prediction method, and addressing a case study. First, several efficiency indicators (the LU value, RQD, and FFR after grouting) are used to comprehensively evaluate the efficiency of curtain grouting. Geological factors (fracture intensity, LU value, and RQD before grouting), effective grouting operation factors (effective grouting pressure, effective grouting time, effective grout volume and effective cement take), as well as tested interval depth, are selected as factors affecting grouting results. Second, a prediction model is established to estimate the efficiency of curtain grouting based on the ANFIS method. The OK and Improved IDW methods are also used to help build the prediction model. Finally, the proposed method is applied to the efficiency of curtain grouting prediction and assessment of a hydropower project in China.

## Curtain grouting efficiency evaluation indicators and the factors affecting grouting results

Curtain grouting efficiency prediction methods try to obtain the relationship between efficiency evaluation indicators and their influencing factors. The prediction systems quantify the efficiency of curtain grouting that is a function of the factors affecting grouting results. This function is generally considered to be nonlinear due to the complexity of the grouting problem. Curtain grouting efficiency, denoted as EI, can thus be defined as a mathematical function ( $f$ ) of the influencing factors ( $f_1, f_2, f_3, \dots, f_n$ ), expressed as Eq. 1.

$$\text{EI (LU, RQD, FFR)} = f(f_1, f_2, f_3, \dots, f_n) \quad (1)$$

### Curtain grouting efficiency evaluation indicators

Curtain grouting programs are designed to construct a seepage cutoff wall, a comparatively watertight and low permeability barrier (Roman et al. 2013). Successful curtain grouting ought to be excellent in both permeability and

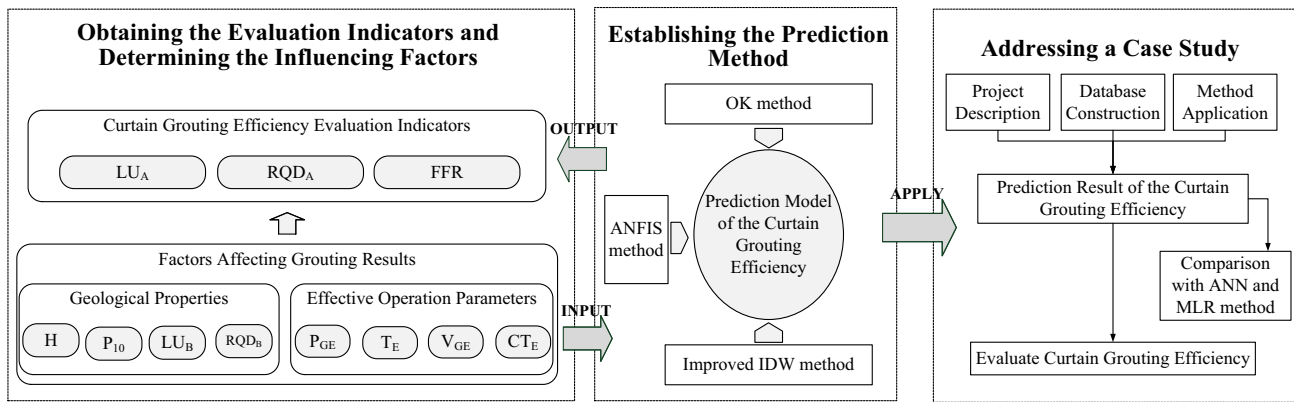


Fig. 1 Research framework

watertightness. This paper evaluated grouting efficiency comprehensively by considering the two perspectives of permeability and watertightness. Therefore, the evaluation indicators of curtain grouting efficiency are the LU value, RQD, and FFR based on the results of WPTs, drilling and coring, and borehole television imaging.

*Lugeon value*

The water pressure test (WPT) or Lugeon test, as introduced by Lugeon (Ewert 1997), is the most popular method used to determine rock mass permeability in curtain grouting effectiveness assessment. According to Lugeon (1933), WPT results are expressed in terms of their Lugeon value (LU). Equation 2 is the definition of the Lugeon value.

$$LU = \frac{Q}{P \cdot L} (L/m/min) \tag{2}$$

where LU is the Lugeon value (Lu); *Q* is the flow rate (L/min); *P* is the effective pressure in the tested segment (MPa); *L* is the length of the studied segment (m).

The LU value is the best physical parameter to express the status of discontinuities in a dam foundation. When the grout improvement is finished, the LU values from WPT verification holes can provide a direct indication of residual permeability (Roman et al. 2013), and the change in LU values is used to assess the efficiency of the grout improvement.

*Rock quality designation*

Rock quality designation was first introduced in 1962 by Deere as the percentage of total length of core pieces longer than 100 mm (*L<sub>i</sub>*) to the total length of the core run (*L*) (Deere 1962). It is expressed as follows in Eq. 3 and Fig. 2.

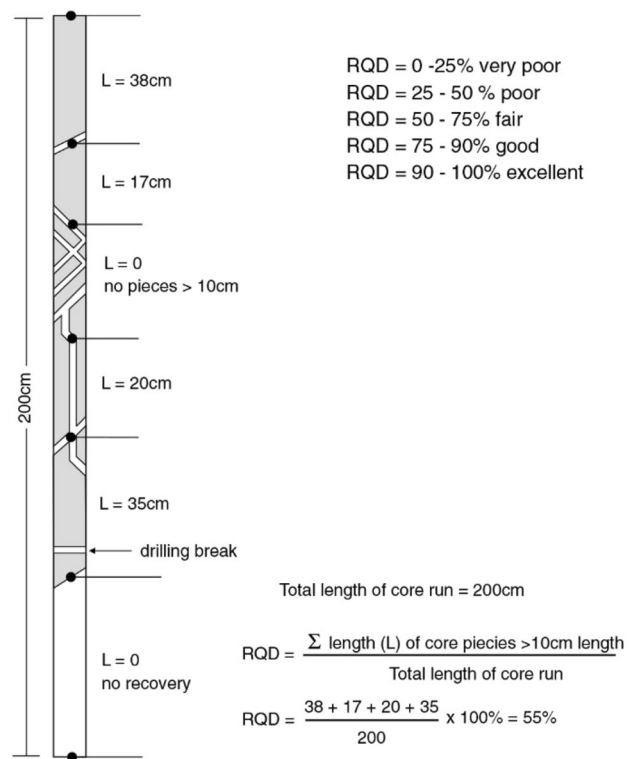


Fig. 2 Procedure for measurement and calculation of RQD (Palmstrom 2005)

$$RQD = \frac{\sum L_i}{L} \times 100\% \tag{3}$$

RQD is perhaps the most commonly used parameter for characterizing the jointing system of a rock mass (Azimian and Ajalloeian 2015). The relationship between the engineering quality of a rock mass and RQD, as proposed by Deere (1968), is very poor (0–25), poor (25–50), fair (50–75), good (75–90), or excellent (90–100).

RQD will be improved due to grouting. Changes in the RQD are attributed to the effect of penetration of cement

into discontinuities in the rock mass. Cement penetrates into the discontinuities, joins the rock pieces together, and consequently increases the RQD value (Zolfaghari et al. 2015).

*Fracture filled rate*

Fracture filled rate is the ratio of the fractures filled by grout (Fan et al. 2016) and can be calculated by Eq. 4, as shown in Fig. 3.

$$FFR = \frac{N_{filled}}{N_{all}} \times 100\% \tag{4}$$

where  $N_{filled}$  is the number of fractures filled by grout;  $N_{all}$  is the total number of fractures in one tested interval.

FFR is used directly to determine how many fractures and voids have been filled by grout. Because it is very intuitive and effective, FFR is commonly used to verify the result of fractures filled by grout and the penetration length by visual observation (Funehag and Fransson 2006).

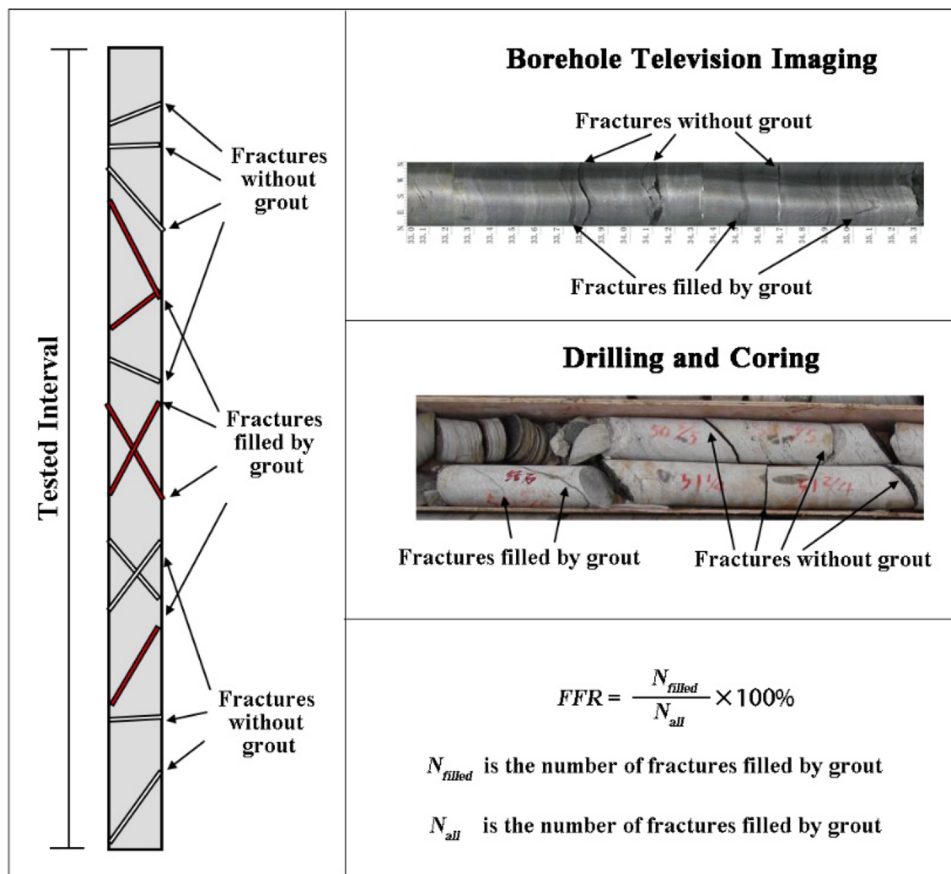
Permeability (LU values), which is assessed from WPTs, as well as RQD and FFR, which are derived from drilling and coring and borehole television imaging, are key parameters in the assessment of grouting efficiency. Low LU values may not reflect high grouting efficiency

because the RQD or FFR may be very low. Only the combination of low LU values, high RQD and high FFR indicate high grouting efficiency.

**Factors affecting grouting results**

In discussions of the relationship between sealing efficiency and the factors that influence it, many researchers have focused on the mechanisms of grouting and sealing in fractured rock masses from both practical and theoretical perspectives. Mortazavi and Maadikhah (2016) argued that grout penetration is one of the most important factors determining the final effect of grouting. Hässler et al. (1992b) and Gustafson and Stille (1996) calculated the maximum grout penetration for a Bingham fluid flow using a shear force balance, which is controlled by factors such as pressure, grout properties, and the joint aperture. Funehag and Fransson (2006) and Funehag and Gustafson (2008a, b) assessed the penetration of grout, taking into consideration the hydraulic aperture, grouting pressure and time, as well as the material characteristics of the grout. Through experiments, a relationship between diffusion radius and grouting pressure, grout viscosity, and grouting time was obtained (Yang et al. 2001). Theoretical and numerical models based on stochastic approaches have also

**Fig. 3** Procedure for measurement and calculation of FFR



been developed to simulate grout propagation in fracture networks by Yang et al. (2002). To demonstrate the effects of the various parameters on grout penetration, sensitivity studies were carried out. The parameters include the characteristics of the fracture (intensity, width, orientation, and length); grout pressure; and the material properties of the grout (initial shear strength and viscosity). Through the use of a model of grout diffusion in a single layer fracture, the diffusion radius of grout as a function of different fracture depths was obtained by Hu (2005). Saeidi et al. (2013) proposed a numerical model to predict grout flow and penetration length into the jointed rock mass using Universal Distinct Element Code, UDEC. The effect of rock mass properties as joint hydraulic aperture, roughness, spacing, trace length, dipping, and grout properties as yield value, viscosity, and grout pressure were considered in grout flow rate and penetration length. Xu et al. (2013) proposed a new empirical formula for diffusion radius by using a multivariate nonlinear fitting analysis based on the mean of values from four empirical formulas, in which the influencing factors are grouting pressure, grouting time, the permeability coefficient and the grout viscosity. Based on the Bingham fluid model, Mortazavi and Maadikhah (2016) investigated the effect of different factors on grout flow analytically and numerically. The results of this analysis show that grout penetration is related to characteristics of the fracture such as aperture, spacing, orientation, normal stiffness, in situ stress, and pore water pressure, as well as operating parameters such as grouting pressure and grout yield stress. According to these studies, numerous factors affect grouting efficiency. In general, the parameters influencing the grouting process can be categorized into two groups: geological factors, including the characteristics of the fracture (intensity, width, orientation, length, and roughness), permeability, in situ stress, pore water pressure and depth, and grouting operation factors, including grouting pressure, grouting time, and properties of the grout (initial shear strength and viscosity), grout consumption and cement take.

It is too difficult to estimate the results of grouting given the complexity of geological conditions and engineering operations, as well as the uncertain relationships between the grouting results and influence factors. Moreover, since some factors may have combined effects, it is not possible to define clearly the role of each factor. For this complex problem, the more influence factors considered, the closer it gets to the actual situation. However, in practice, obtaining values of all factors that influence grouting efficiency is too difficult for a special grouting engineering project, because of the difficulty in obtaining values of factors by field tests, lack of experimental data, or poor reliability of the data. The influence factors of grouting efficiency investigated are not exactly

the same for different engineering with different geological conditions, as can be found in different studies. Azimian and Ajalloeian (2015) evaluated groutability at the Nargesi dam site using secondary permeability index, joint hydraulic aperture, and LU value. In the research of Sadeghiyeh et al. (2013), the permeability (LU value and secondary permeability index), RQD, and cement take values of the Ostur dam site were presented and analysed. The grout volume,  $Q$  value, LU value, SPI value, and joint apertures in the Bakhtiari dam site were investigated in the research of Sohrabi-Bidar et al. (2015). In the research of Yang (2004), some factors that can be categorized or quantified (the strata, zone of dam foundation, depth of grout section, injection pressure, and the LU value) were analyzed in grouting process for Li–Yu–Tan dam. Zadhesh et al. (2015) estimated the grouting efficiency of the Cheraghvays dam using permeability, cement take and depth. However, the most influential factors selected for analysis should be same, including permeability, fracture aperture, grouting pressure, and cement take.

Fracture aperture, a key factor in determining groutability and grout penetration, is difficult to obtain or its data are of poor reliability in field investigations. Permeability (LU value) as measured by WPTs is related to the hydraulic aperture. The results of WPTs can characterize the fracture aperture, referring to a series of studies (Fransson 2001; Gustafson 2012; Kvarstberg and Fransson 2013; Lisa et al. 2012). From WPTs, it is possible to evaluate the transmissivity,  $T$  ( $\text{m}^2/\text{s}$ ), which governs the water transport capacity of a rock mass to a specific borehole. The term may also be used as a measure of the ability of a fracture to transmit water (fracture transmissivity,  $T_f$ ). A simple, yet reasonable estimate of the relationship between the transmissivity and the hydraulic aperture  $b$ , is provided using the cubic law (Snow 1968).

$$b = \sqrt[3]{\frac{12\mu_w T}{\rho_w g}} \quad (5)$$

where  $\mu_w$  is the viscosity of water (Pas);  $T$  is the transmissivity of the fracture ( $\text{m}^2/\text{s}$ );  $\rho_w$  is the density of water ( $\text{kg}/\text{m}^3$ ), and  $g$  is the gravitational acceleration ( $\text{m}/\text{s}^2$ ). The cubic law is based on laminar flow and idealises fractures as equivalent parallel plate openings. In addition, the LU value shows the degree of permeability in the dam foundation. Generally, in grout improvement, a dam foundation that has a high LU value requires more cement take. Therefore, permeability (LU value), a comprehensive index that can characterize the fracture, was selected as an important influence factor.

Fracture intensity  $P_{10}$ , also referred to as the lineal fracture intensity, and RQD as measured from core logs,

reflect the characteristics of the fractures as well. The depth is a very important factor that affects grouting efficiency (Hu 2005; Mortazavi and Maadikhah 2016; Yang 2004), owing to that the in situ stress and pore water pressure change with depth. (Note also that as the depth increases, the in-situ stress—which is often estimated by  $\lambda H$  with  $\lambda$  being the unit weight of the rock mass—also increases.) In a rock layers deeper into the underground, the cracks are narrow and comparatively do not take in grout because of the greater tectonic stresses in lower elevation. Although in situ stress and pore water pressure would probably be better predictors, the lack of information about in situ stress and pore water pressure in many projects, as well as the difficulties to accurately estimate them without expensive and time consuming in situ tests, led us to select the depth as an alternative. The operational factors, grouting pressure and grouting time, are easily obtained. For successful improvement of rock masses by grouting, the volume of grout that must be injected in each stage depends on the chosen hole spacing and arrangement, in addition to the formation's geological properties (Carter et al. 2012). Therefore, the grout volume and cement take are important factors in determining the grouting efficiency, and are also selected as inputs to predict grouting efficiency in this paper. Grout parameters such as yield strength and viscosity are important grout parameters influencing grouting efficiency. To obtain a proper water sealing, a desired spread of grout must be achieved and the rheology of the cement grout is the governing factor for estimating the required spread. However, the rheological behavior of cement based grout can be considered complex (Håkansson 1993). Rheological properties of cement grout such as viscosity and yield stress are affected by many factors, such as water–cement ( $w/c$ ) ratio, mixing time, and temperature (Eriksson et al. 2004). The yield stress and viscosity change due to hydration with time (Håkansson 1993). It is too difficult to obtain accurate rheological property values for each grouting process, especially for the grout entering fractures. In this study, the rheological properties of the grout were similar because uniform grout was used for different grouting boreholes in the field grouting operation. Therefore, it was not investigated the influence of the change of grout properties as yield strength and viscosity on the grouting effect, as many other studies deal with the problem in grouting engineering (Azimian and Ajalloeian 2015; Sadeghiyeh et al. 2013; Sohrabi-Bidar et al. 2015; Yang 2004; Zadhesh et al. 2015).

Based on previous studies and data collected from practical engineering projects, geological factors (including permeability, fracture intensity, and RQD before grouting), and grouting operation factors (including grouting pressure, grouting time, grout volume, and cement take during the grouting process), as well as the depth of the tested

interval, are set as model inputs to predict grouting efficiency for a case study in this paper, as shown in Fig. 4.

## Methodology

### Mathematical model of curtain grouting efficiency prediction method

#### *Conceptual model of curtain grouting*

Dam curtain grouting involves forming a curtain to cut off leakage and reduce groundwater flow. Figure 5 shows a common arrangement of boreholes used in curtain grouting. The grouting curtain is composed of two or three rows of boreholes. Drilling begins with the boreholes in the downstream row. The upper row is drilled second, and the middle row last. Boreholes in a row are divided into three orders, primary, secondary, and tertiary boreholes. The spacing between the holes progressively decreases, and each order of boreholes is normally drilled, tested, and grouted before the next order is executed.

Grouting injects cement grout into fractures connected to the grout injection boreholes. The penetration should be deep enough for the critical fractures in the rock between two neighboring boreholes to be filled, hence sealing the rock mass and making it an effective barrier to water flow. Therefore, the efficiency in grouting the fractured rock depends on the penetration of the grout into the individual fractures and its propagation into the connected fracture networks. In another way, the grouting effect of a certain location is influenced by the grouting boreholes within the grout penetration depth. If we know the grout penetration depth and the impact of grouting boreholes within it, then the grouting effect of this point can be evaluated reliably.

#### *Mathematical function of curtain grouting efficiency prediction method*

In this paper, we try to obtain the relationship between efficiency evaluation indicators and their influencing factors. The efficiency of curtain grouting, denoted as EI, can be defined as a mathematical function ( $f$ ) of geological parameters ( $P_{Geo}$ ) and grouting operation parameters ( $P_{Gro}$ ), expressed as Eq. 6. The geological and grouting operation parameter sets are given by Eqs. 7 and 8. The geological parameter set includes depth ( $H$ ), fracture intensity ( $P_{10}$ ), Lugeon value ( $LU_B$ ), and RQD ( $RQD_B$ ) before grouting, and the grouting operation parameter set includes effective grouting pressure ( $P_{GE}$ ), effective grouting time ( $T_E$ ), effective grout volume ( $V_{GE}$ ), and effective cement take ( $CT_E$ ). The effective grouting operation parameters are calculated by the Eq. 9, where  $P_{Gi}$ ,  $T_i$ ,

**Fig. 4** Selected categories and principal factors affecting the grouting efficiency

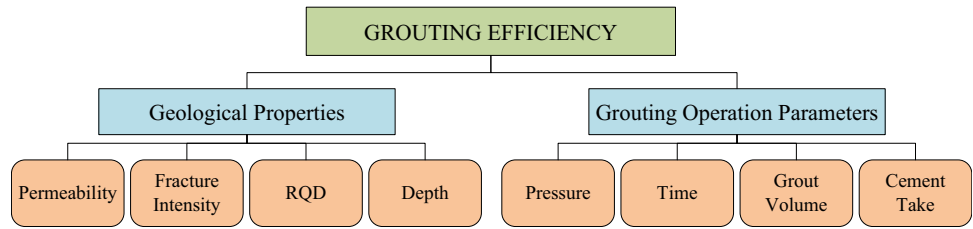
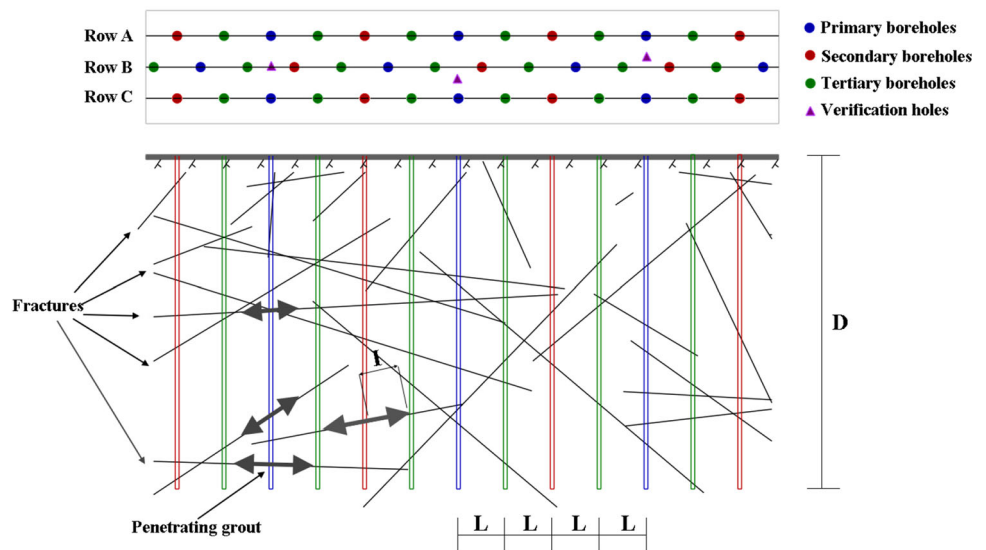


**Fig. 5** Diagram showing curtain grouting in a fractured rock mass



$V_{Gi}$ , and  $CT_i$  are the grouting pressure, time, grout volume, and cement take of the  $i$ th injection interval in adjacent grouting boreholes,  $\oplus$  is a summation operator and  $N$  is the number of grouting intervals within the grouting influence distance.

$$EI(LU, RQD, FFR) = f(P_{Geo}, P_{Gro}) \tag{6}$$

$$P_{Geo} = \{H, P_{10}, LU_B, RQD_B\} \tag{7}$$

$$P_{Gro} = \{P_{GE}, T_E, V_{GE}, C_{TE}\} \tag{8}$$

$$\begin{cases} P_{GE} = P_{G_1} \oplus P_{G_2} \oplus \dots \oplus P_{G_N} \\ T_E = T_1 \oplus T_2 \oplus \dots \oplus T_N \\ V_{GE} = V_{G_1} \oplus V_{G_2} \oplus \dots \oplus V_{G_N} \\ CT_E = CT_1 \oplus CT_2 \oplus \dots \oplus CT_N \end{cases} \tag{9}$$

**A formula for estimating grouting influence radius based on cement take of grouting boreholes**

In practice, the grouting process is carried out in sequence: previous boreholes are normally drilled, tested, and grouted before the next boreholes are executed, with the advantage that the effect of grouting of the previous boreholes may be controlled by the new boreholes positioned next to them. In general, the permeability and grout volume/cement take of the second boreholes are lower than those of the first

boreholes due to the grouting of the first boreholes. Therefore, the penetration distance can be estimated by the cement take or permeability change of two grouting boreholes drilled in sequence. In this paper, a formula for estimation of the grouting influence radius based on the cement take of grouting boreholes is proposed.

Figure 6 illustrates the results of grout diffusion in two adjacent grouting boreholes which are successively grouted. This grouting process is carried out in sequence; G-1A is grouted first and G-1B is grouted later. If the distance between boreholes G-1A and G-1B is great enough that they have no influence on each other, grout is then injected into fractures intersecting each borehole until the fractures are completely grouted or a specified maximum depth of grout penetration is reached. Assuming they encounter the same geological conditions, the grout-filled volume of the two boreholes should be almost equal. However, if the penetration distance in the fractures is more than half the distance between the boreholes, grout from the first borehole, G-1A, fills fractures connected to the subsequent borehole, G-1B, and those fractures cannot accept more grout. Thus, the grouting for borehole G-1B is less than the grout-filled volume of borehole G-1A calculated based on the grout penetration.

The vertical section and plan view help to illustrate the problem better. The pattern of grout propagation along the



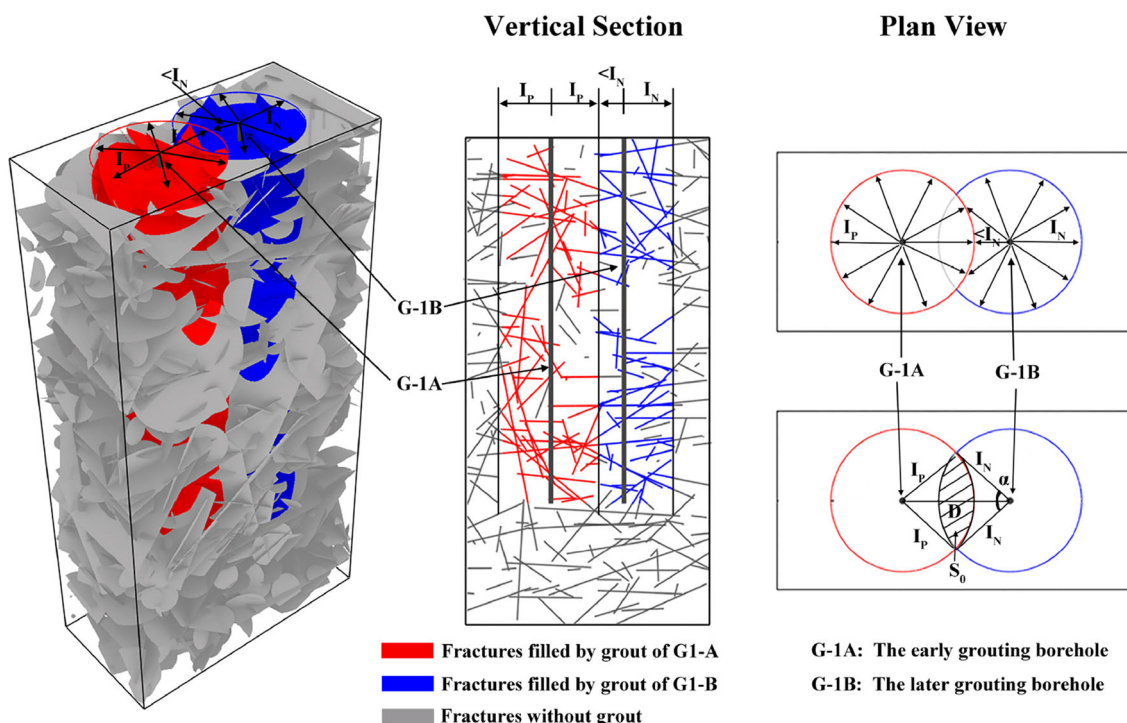


Fig. 6 Sketch of the conceptual grout diffusion model of two adjacent grouting boreholes

boreholes is shown in the vertical section. Red lines are fractures filled by grout from borehole G-1A, and blue lines are related to the grouting of borehole G-1B. The fractures within the zone of overlap between the two boreholes are preferentially filled with grout from borehole G-1A and will not be further grouted by borehole G-1B. This figure shows that the grouting of first borehole affects the grouting of the second borehole. The overlap of the two boreholes is more intuitive in plan view.

To establish a mathematical model of grouting influence radius estimation, some hypotheses are necessary. (1) The grout is diffused in the form of a column in the fractured rock mass. (2) The fractures are uniformly distributed throughout the rock mass.

Based on the grouting model in Fig. 6 and the hypotheses above, the grout-filled volume associated with a borehole is:

$$V_g = V_I \cdot P_{33} \cdot P_C \cdot P_F \tag{10}$$

where  $V_I$  is the rock mass volume penetrated by grout;  $P_{33}$  is the fracture porosity parameter, which refers to the volume of fractures per unit volume of rock mass;  $P_C$  is the fracture network connectivity parameter, which refers to the percentage of fracture volume connected with the grouting hole;  $P_F$  is the grout filling parameter, which refers to the percentage of volume being filled with grout.

The ratio of grout-filled volume of the two grouting boreholes is:

$$R_{N-P} = \frac{V_{gN}}{V_{gP}} \tag{11}$$

where  $V_{gP}$  is the grout-filled volume of the previous borehole, and  $V_{gN}$  is the grout-filled volume of the next borehole.

$$V_{gP} = V_{IP} \cdot P_{33} \cdot P_C \cdot P_F \tag{12}$$

$$V_{gN} = V_{IN} \cdot P_{33} \cdot P_C \cdot P_F \tag{13}$$

where  $V_{IP}$  is the rock mass volume penetrated by grout from the previous borehole;  $V_{IN}$  is the rock mass volume penetrated by grout from the next borehole. Obviously, the following equation can then be obtained:

$$R_{N-P} = \frac{V_{IN}}{V_{IP}} = \frac{a_0 \cdot CT_N}{a_0 \cdot CT_P} = \frac{CT_N}{CT_P} \tag{14}$$

where  $CT_P$  is the cement take of the previous borehole;  $CT_N$  is the cement take of the next borehole;  $a_0$  is a parameter related to the grout gel properties.

By using appropriate geometric relationships and the grouting model presented in Fig. 6, the following equations can be obtained:

$$V_{IP} = \pi I_P^2 \cdot L \tag{15}$$

$$V_{IN} = (\pi I_N^2 - S_O) \cdot L \tag{16}$$

$$S_O = \alpha I_N^2 - I_N^2 \sin \alpha \tag{17}$$

where  $I_P$  is the grouting influence radius of the previous borehole;  $I_N$  is the grouting influence radius of the next borehole;  $L$  is the grouting interval length;  $S_O$  is the area of overlap in plan view;  $\alpha$  is the central angle of the area of overlap of the previous borehole.

Combining Eqs. 14–17, the following relationship can be obtained:

$$R_{N-P} = \frac{\pi - \alpha + \sin \alpha}{\pi} \left( \frac{I_N}{I_P} \right)^2 \tag{18}$$

A cement-based grout can be described as a Bingham fluid characterized by a viscosity and a yield stress. At the point of refusal, the injection pressure is balanced by the shear stress towards the fracture walls. The max grout penetration,  $I_{max}$ , in a parallel slot with aperture  $b$  can thus be calculated to be (Gustafson and Stille 1996):

$$I_{max} = \frac{P_g - P_w}{2\tau_0} b \tag{19}$$

where  $P_g - P_w = \Delta P$  is the difference between the injection and ground-water pressures and  $\tau_0$  is the yield stress of the grout. As can be seen in Eq. 19, the max grout penetration depends on the grouting pressure, fracture aperture and the yield strength of grout. Therefore, we obtain:

$$\frac{I_N}{I_P} = \frac{\Delta P_N b_N \tau_{0P}}{\Delta P_P b_P \tau_{0N}} \tag{20}$$

where  $\Delta P_P$  and  $\Delta P_N$  are the differences between the injection and ground-water pressures for the previous borehole and the next borehole respectively;  $b_P$  and  $b_N$  are fracture apertures for the previous borehole and the next borehole respectively;  $\tau_{0P}$  and  $\tau_{0N}$  are yield strengths of grout for the previous borehole and the next borehole respectively. Assuming that these three parameters are equal, the grouting influence radius of the previous borehole is equal to the grouting influence radius of the next borehole.

$$I_P = I_N = I \tag{21}$$

where  $I$  is the grouting influence radius. Then, Eq. 18 becomes:

$$\alpha - \sin \alpha = (1 - R_{N-P})\pi \tag{22}$$

The distance between the two boreholes,  $D$ , is:

$$D = 2I \cdot \cos \frac{\alpha}{2} \tag{23}$$

Finally, the grouting influence radius is:

$$I = \frac{D}{2 \cos \frac{\alpha}{2}} \tag{24}$$

Since Eq. 22 is a transcendental equation, graphical methods may provide the best solution, although they are approximate. Combining Eqs. 22 and 24 with graphical methods, Fig. 7 provides a query curve which can help us to obtain quickly the corresponding ratio ( $I/D$ ) of the grouting influence radius and the distance between two boreholes based on the ratio of grout-filled volume of the two grouting boreholes ( $R_{N-P}$ ).

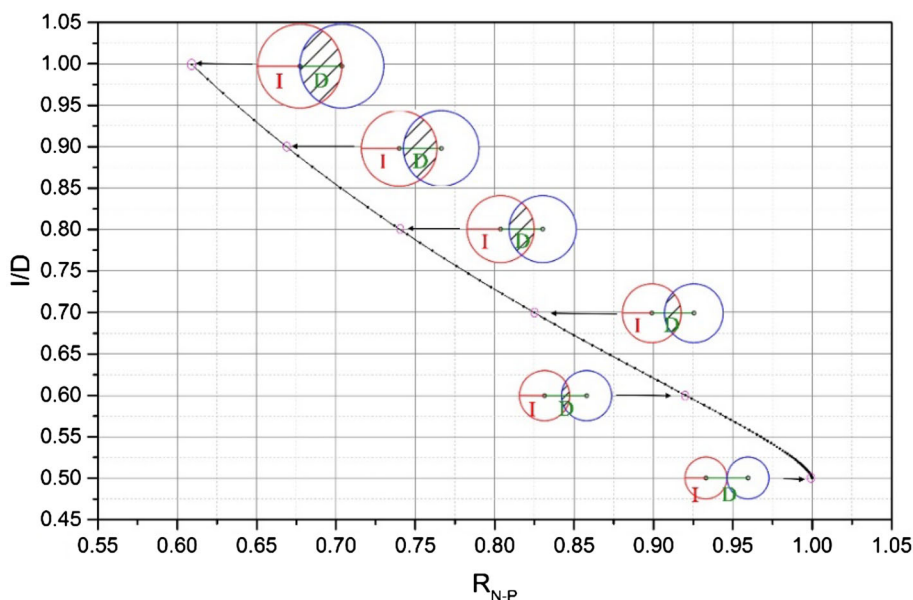
### Improved inverse distance weighting method for estimating the effective grouting operation parameters

The grouting operation factors, including grouting pressure, grouting time, grout volume, and cement take during the grouting process, are major technical factors affecting grouting effect. However, the values of these parameters are all recorded for particular grouting intervals, and can even be considered point data in specific locations. The collected data do not tell us what is occurring between them. The grouting effect, which is influenced by the injection interval of adjacent grouting boreholes within the distance of grouting influence, is not only related to the grouting operation parameters of these holes, but is also strongly influenced by their spatial relationships. Considering that the diffusion distance of grout in the rock mass is limited and that the arrangement of grouting boreholes is based on the grout diffusion distance, it is assumed that the grouting effect at a certain point is only influenced by the surrounding grouting interval and that large grouting intervals lead to weak effects due to the long distance. To solve this problem, incorporating the grouting operation factors of boreholes and the spatial relationships between verification holes or points of concern and grouting boreholes, several effective grouting operation parameters are proposed in this paper. These parameters include the effective grouting pressure ( $P_{GE}$ ), effective grouting time ( $T_E$ ), effective grout volume ( $V_{GE}$ ), and effective cement take ( $CT_E$ ) and are estimated based on an improved IDW method.

The IDW method is one of the most frequently used deterministic models in spatial interpolation and is based on the assumption that the value of an unsampled point is the weighted average of known values within the neighborhood, and the weights are inversely related to the distances between the prediction location and the sampled locations (Lu and Wong 2008). The IDW formulas are given as Eqs. 25 and 26.

$$Z_p = \sum_{i=1}^N \omega_i Z_i \tag{25}$$

**Fig. 7** The ratio of the grouting influence radius and the distance between the two grouting boreholes ( $I/D$ ) as a function of the ratio of grout-filled volume of the boreholes ( $R_{N-P}$ )



$$\omega_i = \frac{d_i^{-\mu}}{\sum_{i=1}^N d_i^{-\mu}} \tag{26}$$

where  $Z_p$  indicates the value at the prediction location  $X_p$ ;  $Z_i$  indicates the known value at sampled point  $X_i$ ;  $N$  indicates the number of known values within the search radius;  $\omega_i$  indicates the weighting of each point within the neighborhood;  $d_i$  indicates the distance from each point to the unknown point;  $\mu$  indicates the power, and is also a control parameter.

For estimating the effective grouting operation parameters in this paper, the traditional IDW method is not suitable, because the grouting process is carried out in sequence where grouting boreholes of different orders are alternately arranged. The parameters such as grout volume and cement take may differ strongly depending on the sequence in which the boreholes are grouted. Therefore, IDW, which assumes that the attribute value of an unsampled point is the weighted average of known values within the neighborhood, should be improved accordingly. In this paper, an improved IDW method is proposed by modifying the weight formula of Eq. 24. The improved weight formula is as follows:

$$\omega_i = d_i^{-\mu} \tag{27}$$

The improved method reflects the insight that the value of an unsampled point is the weighted sum of known values within the neighborhood, instead of the average. Then, the effective grouting operation parameters are calculated by combining the values recorded for different

grouting intervals within the search radius ( $R$ ) using the improved IDW, as defined in Eqs. 28–32:

$$P_{GE} = \sum_{i=1}^N \omega_i P_{Gi} \tag{28}$$

$$T_E = \sum_{i=1}^N \omega_i T_i \tag{29}$$

$$V_{GE} = \sum_{i=1}^N \omega_i V_{Gi} \tag{30}$$

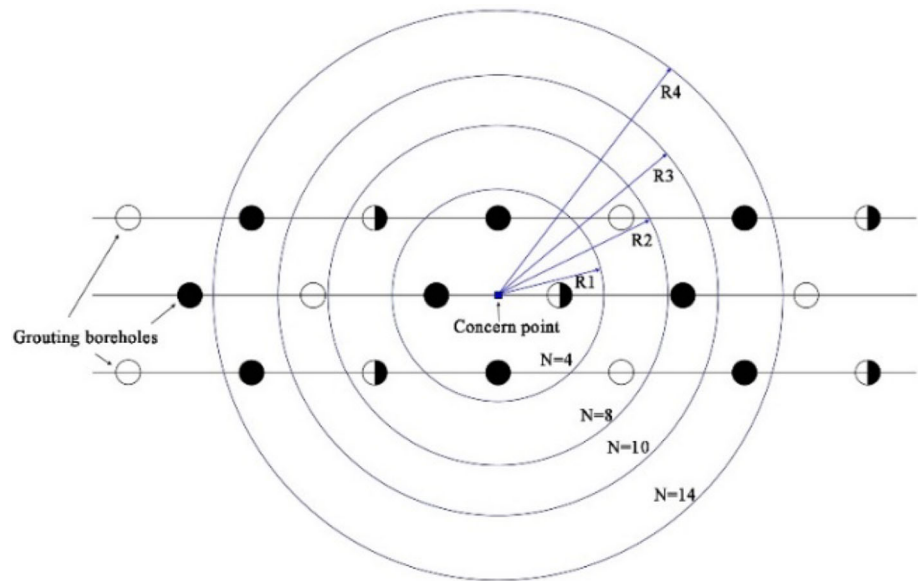
$$CT_E = \sum_{i=1}^N \omega_i CT_i \tag{31}$$

$$\omega_i = d_i^{-\mu}, \quad i \in \Omega_R \tag{32}$$

where  $P_{Gi}$ ,  $T_i$ ,  $V_{Gi}$ , and  $CT_i$  are the grouting pressure, time, grout volume and cement take of the  $i$ th injection interval in adjacent grouting boreholes;  $\Omega_R$  is the grouting region within the grouting influence distance.

In addition, to improve the interpolation accuracy of IDW for a specific problem, the power ( $\mu$  value) and search radius ( $R$ ) must be chosen properly. The search radius ( $R$ ) is the most important parameter, because it determines the number of grouting boreholes that have an effect on a certain point. As seen in Fig. 8, differing numbers of grouting boreholes lie within different influence radius values. For the problem of predicting curtain grouting efficiency,  $\mu$  is assigned as 1 in this paper, and this choice should be investigated further in the future. The search radius or influence radius ( $R$ ) is used as

**Fig. 8** Distribution of grouting boreholes within the influence radius of the point of concern



the grouting influence radius, and this choice is discussed in the previous section.

### Ordinary Kriging (OK) method for estimating geological properties

In this paper, geological properties, including permeability, fracture intensity, and RQD of the rock mass before grouting are used as prediction model inputs to predict grouting efficiency and are the key influence factors affecting grouting effect. However, it is a common practice to execute in situ tests at a few representative locations, reducing time and costs. In engineering applications, common techniques for measuring rock mass properties provide point values that refer to a specific sampling location (Ferrari et al. 2014). At the same, the permeability, fracture intensity, and RQD values of rock mass before grouting are carried out using samples taken from drill hole investigations, which are spatially discrete point data. The distribution of geological properties cannot be obtained for the whole area even if the location we are concerned with or the verification holes are carefully chosen.

Therefore, indirect techniques, such as geostatistical methods, have been suggested to estimate rock mass characteristics over large areas. Several studies have applied the geostatistical approach to determine the specific properties of rock masses. Ahmed and De Marsily (1987), Razack and Lasm (2006), and Akhondi and Mohammadi (2014) used geostatistical methods for estimating rock mass permeability. Long and Billaux (1987), Chiles (1988) and Rafiee and Vinches (2008), applied geostatistical approaches to analyze the distribution of fractures within rock masses. Ztürk and Nasuf (2002) and Ozturk and Simdi

(2014) proposed the use of geostatistical applications to estimate RQD. Based on the cited literature, this paper uses geostatistical methods to estimate the geological properties of permeability, fracture intensity, and RQD of the rock mass before grouting.

### Adaptive neuro-fuzzy inference system methods

The ANFIS method, first introduced by Jang (1993), combines an adaptive neural network with a fuzzy inference system. This system is capable of approximating any real continuous function on a compact set to any degree of accuracy. Therefore, a functional mapping can be modeled by ANFIS that approximates the prediction process of the internal system parameters. ANFIS has been extensively used in the field of geotechnical engineering (Ehsanzadeh and Ahangari 2014; Jahed Armaghani et al. 2015; Kayabasi et al. 2015; Kucuk et al. 2011; Singh et al. 2012).

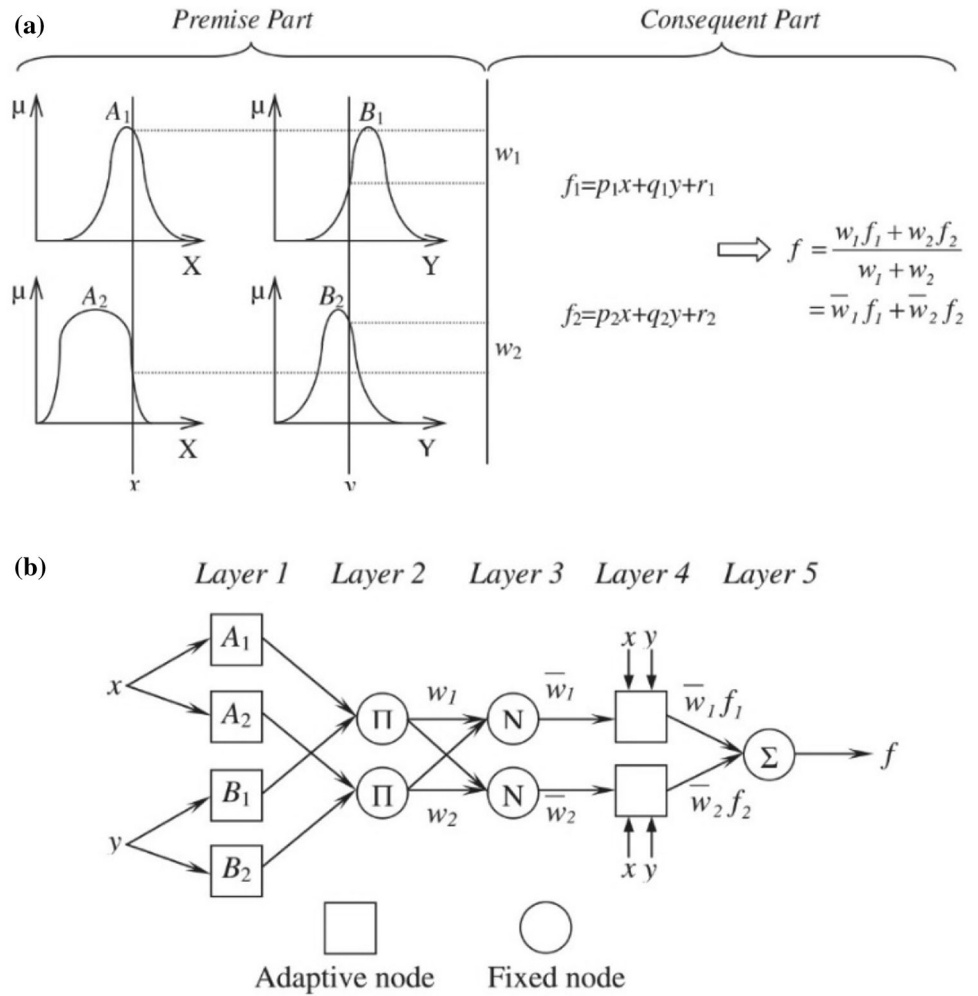
The ANFIS used in this study is the first-order Sugeno fuzzy model (Jang 1993; Oh and Pradhan 2011; Takagi and Sugeno 1983). Figure 9 shows the architecture of a typical ANFIS with two inputs ( $x, y$ ), two rules, one output ( $f$ ), and five layers. Each layer involves several nodes, which are described by the node function.

Each input is assumed to have two associated membership functions (MFs). Two fuzzy “if–then” rules can be constructed as follows:

$$\text{Rule 1: if } x \text{ is } A_1 \text{ and } y \text{ is } B_1, \quad \text{then } f_1 = p_1x + q_1y + r_1 \quad (33)$$

$$\text{Rule 2 : if } x \text{ is } A_2 \text{ and } y \text{ is } B_2, \quad \text{then } f_2 = p_2x + q_2y + r_2 \quad (34)$$

**Fig. 9** **a** A two-input first-order Sugeno fuzzy model with two rules; **b** architecture of ANFIS (Jang 1993)



where  $A_1, A_2, B_1,$  and  $B_2$  are the MFs for the inputs  $x$  and  $y$ , and  $p_1, q_1, r_1, p_2, q_2,$  and  $r_2$  are consequent parameters. The descriptions and characteristics of the different layers are given below.

**Layer 1:** all the nodes in this layer are adaptive nodes. The first layer of ANFIS accepts crisp values as inputs and converts them to memberships. In other words, it is responsible for fuzzification and contains as many neurons as the total number of fuzzy sets. They generate membership grades for the inputs. The outputs of this layer are given by

$$O_{A_i}^1 = \mu_{A_i}(x), \quad i = 1, 2 \tag{35}$$

$$O_{B_i}^1 = \mu_{B_i}(y), \quad i = 1, 2 \tag{36}$$

where  $x$  and  $y$  are crisp inputs and  $A_i$  and  $B_i$  are fuzzy sets, such as low and high values characterized by appropriate MFs of  $\mu_{A_i}$  and  $\mu_{B_i}$ , which could be triangular, trapezoidal, or Gaussian functions, generalized bell curves, or other shapes.

**Layer 2:** the nodes in this layer are fixed nodes labeled as  $\Pi$ . Each node output represents the firing strength of a rule, whose output is the product of all inputs:

$$O_i^2 = \omega_i = \mu_{A_i}(x)\mu_{B_i}(y), \quad i = 1, 2 \tag{37}$$

where  $\omega_i$  represents the firing strength of a rule.

**Layer 3:** the nodes in this layer are also fixed nodes labeled as  $N$ . The outputs of this layer are called normalized firing strengths as follows:

$$O_i^3 = \bar{\omega}_i = \frac{\omega_i}{\omega_1 + \omega_2}, \quad i = 1, 2 \tag{38}$$

**Layer 4:** each node in this layer is an adaptive node, whose output is simply the product of the normalized firing strength and a first-order polynomial.

$$O_i^4 = \bar{\omega}_i f_i = \bar{\omega}_i(p_i x + q_i y + r_i), \quad i = 1, 2 \tag{39}$$

where parameters  $p_i, q_i,$  and  $r_i$  are named as consequent parameters.

Layer 5: the single node in this layer is a fixed node labeled with  $\sum$ , which computes the overall output as the summation of all incoming signals.

$$O_1^5 = \sum_i \bar{\omega}_i f_i = \frac{\sum_i \omega_i f_i}{\sum_i \omega_i} \tag{40}$$

The advantage of using the ANFIS model is that the consequent parameters and optimal premise parameters can be efficiently obtained in the learning process (Jahed Armaghani et al. 2015). Similar to the ANN procedure, the system errors are propagated back and the parameters are updated using the gradient descent in the backward pass. Subsequently, the final output can be defined as follows:

$$f = \frac{\omega_1 f_1 + \omega_2 f_2}{\omega_1 + \omega_2} = \bar{\omega}_1(p_1x + q_1y + r_1) + \bar{\omega}_2(p_2x + q_2y + r_2) \tag{41}$$

### Prediction of the evaluation indicators of curtain grouting efficiency based on ANFIS

In this paper, prediction models for curtain grouting efficiency evaluation indicators based on ANFIS are proposed to solve the problem of predicting the results of grouting. As previously discussed, curtain grouting efficiency evaluation indicators depend on the set of grouting operation parameters and on the geological properties of the rock

mass. For this paper, three ANFIS models were designed using the Matlab neural network toolbox. In addition, the structure of the designed ANFIS models can be seen in Fig. 10. Each network consists of an input layer with eight neurons standing for the depth of the tested interval, fracture intensity, LU value, RQD before grouting, effective grouting pressure ( $P_{GE}$ ), effective grouting time ( $T_E$ ), effective grout volume ( $V_{GE}$ ), and effective cement take ( $CT_E$ ) during the grouting process; an input MFs layer; a rules layer; an output MFs layer and an output layer with one output from each model for the LU value, RQD, or FFR. In this study, many attempts have been made to choose the optimal ANFIS structure by changing the training options in the ANFIS algorithm.

Figure 11 shows a flow chart for predicting and evaluating curtain grouting efficiency using the ANFIS modeling and spatial data flow diagram. This procedure mainly consists of three steps, database construction, ANFIS construction and training, and evaluation of curtain grouting efficiency. The database includes input and output data and is also randomly divided into training and test data sets. It uses the OK method to calculate the values of geological factors, including permeability, fracture intensity, and RQD before grouting. For the effective grouting operation factors, first, the influence radius of the grouting borehole is estimated using the method proposed in the previous section, and then the effective grouting pressure ( $P_{GE}$ ), effective grouting time ( $T_E$ ), effective grout volume ( $V_{GE}$ ), and effective cement take ( $CT_E$ ) are calculated by the improved IDW method, which better reflects the influence of other grouting holes on characteristics at the position of interest. The evaluation indicators of curtain grouting efficiency, including the LU value, RQD, and FFR after grouting, are obtained from WPTs, borehole TV, and coring. The prediction model based on ANFIS is designed to map the relationship between effectiveness indicators and influence factors by training using the training data set and is validated using the test data set. Finally, using the prediction models for curtain grouting efficiency evaluation indicators based on ANFIS, the improvement in dam foundation properties after grouting can be predicted. Then, the grouting efficiency is evaluated based on the prediction results, which are obtained in advance.

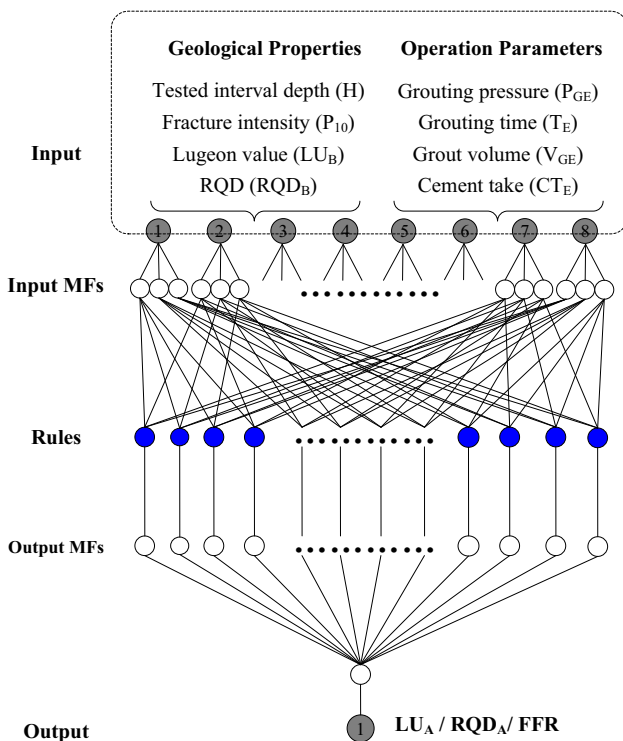


Fig. 10 ANFIS structure for prediction of curtain grouting efficiency evaluation indicators

### Case study

The ANFIS-based prediction models have been applied to a case study to predict the efficiency of curtain grouting for hydropower project A, a large hydropower station constructed on the Jinsha River between the Yunnan province and Sichuan province, southwest of China, as shown in Fig. 12. Hydropower project A, which includes a concrete

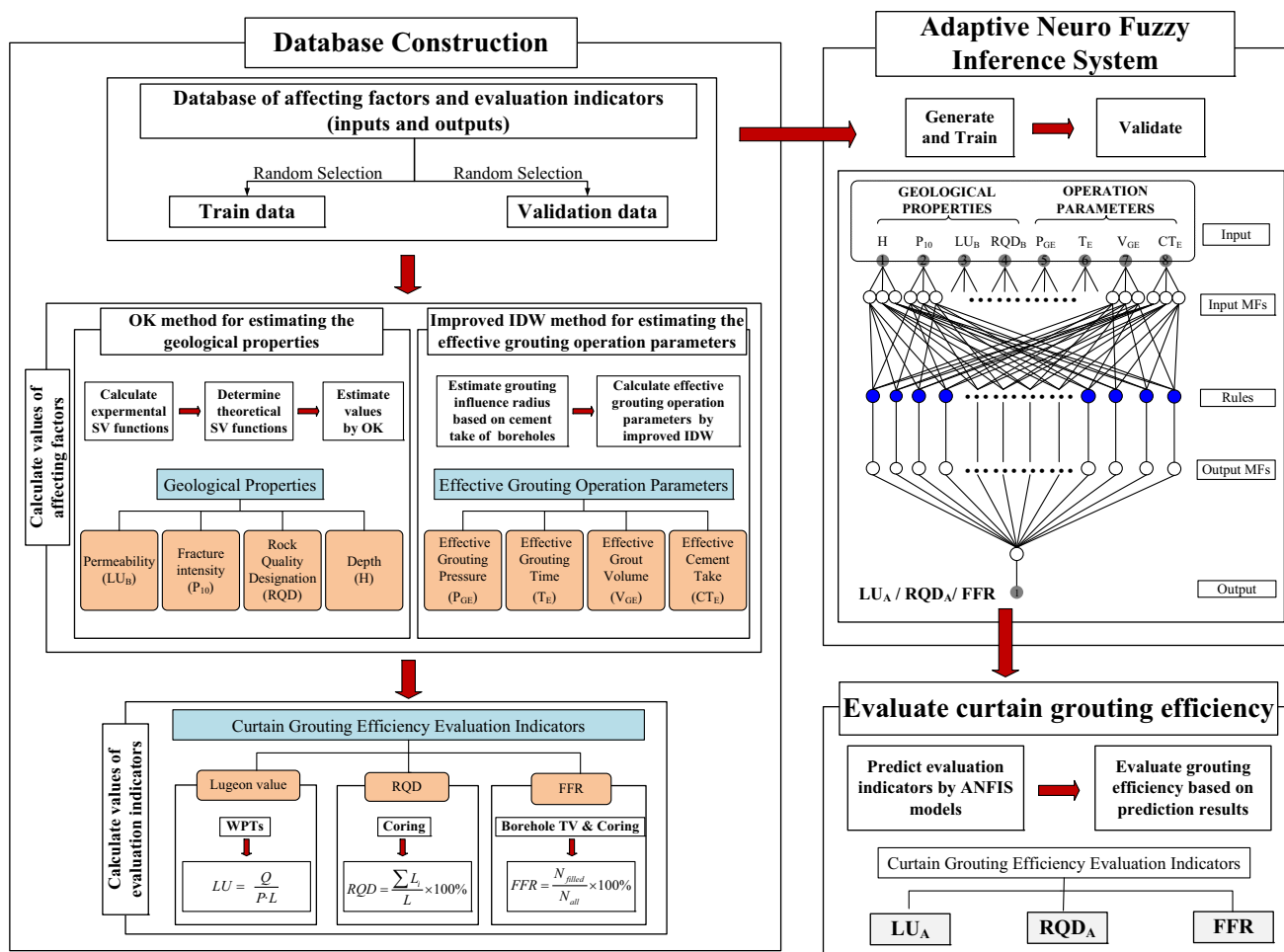


Fig. 11 Flow chart for predicting and evaluating curtain grouting efficiency using the ANFIS-based model and spatial data flow diagram

gravity dam, a spillway, a powerhouse, an underground powerhouse, and a ship lift, is mainly designed to generate electricity. It also improves navigation conditions, controls flooding, provides irrigation water, and regulates the flow of water downstream (Huo et al. 2015; Yan 2014).

**Description of curtain grouting**

The dam site is located in the eastern portion of the Tangfangwan anticline, and the Limeiwan deflection, a knee shaped deflection, extends through it (Huo et al. 2015; Yan 2014). These structures result in complicated geological properties at the dam’s foundation. To improve the dam foundation by decreasing permeability and enhancing the strength of the rock mass, a large number of curtain grouting boreholes have been designed and carried out. As shown in Fig. 13, there are five main grouting curtains arranged along the dam grouting galleries, including the upstream, downstream, left abutment, right abutment, and stilling basin grouting curtains. These curtains extend deep into the rock foundation.

According to the design requirements of curtain grouting, it is carried out sequentially, with three rows (downstream, upstream, middle) and three orders (I, II, III) in each row. The downstream row is constructed first, then the upstream row, and finally the middle row. The grouting boreholes are divided into intervals that are generally 5 m and are grouted from the top down. The process of grouting in each interval is arranged in the following sequence: drilling, washing, water testing, and grouting. Once grouting has been completed in a given area, neighboring verification holes are made and in situ tests, such as WPTs, are carried out in them to verify the effects of grouting. There are numerous grouting units in this project. All of the data were collected by a real-time analysis and feedback system (Zhong et al. 2015), which was applied to hydro-power project A during the curtain grouting construction process. In this paper, nine units are selected from the upstream grouting curtain of the powerhouse section, outlined by the blue box showing the study region in Fig. 13, to build the prediction models and then predict the grouting efficiency.

**Fig. 12** Location of hydropower project A

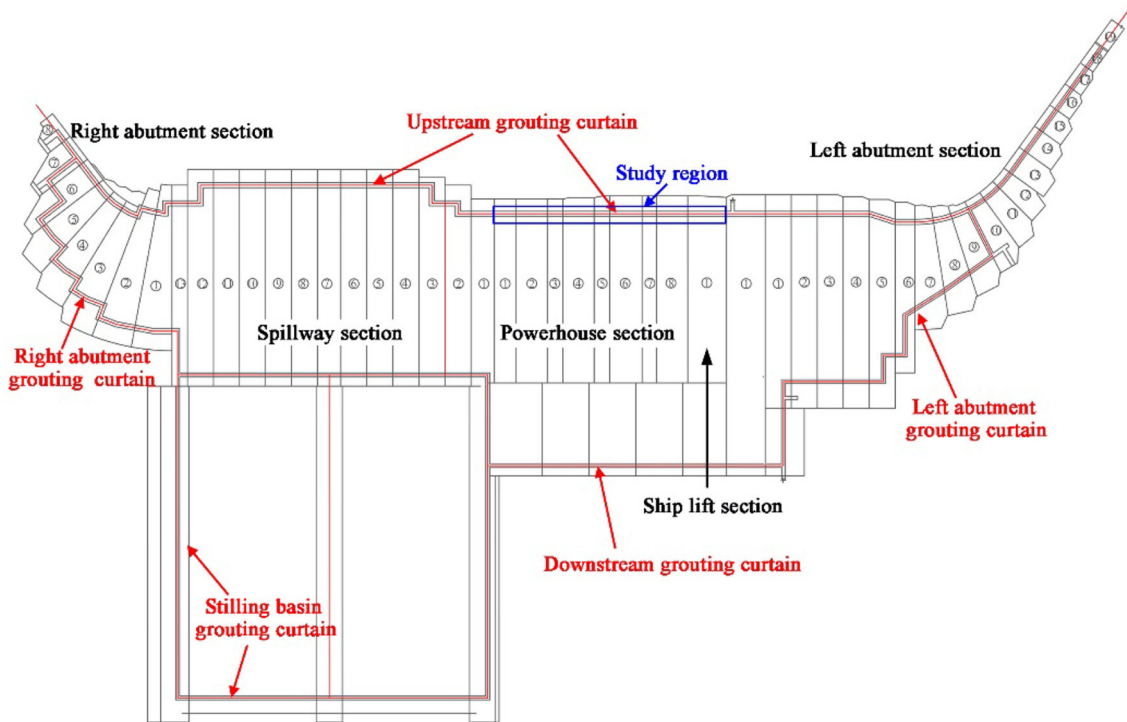
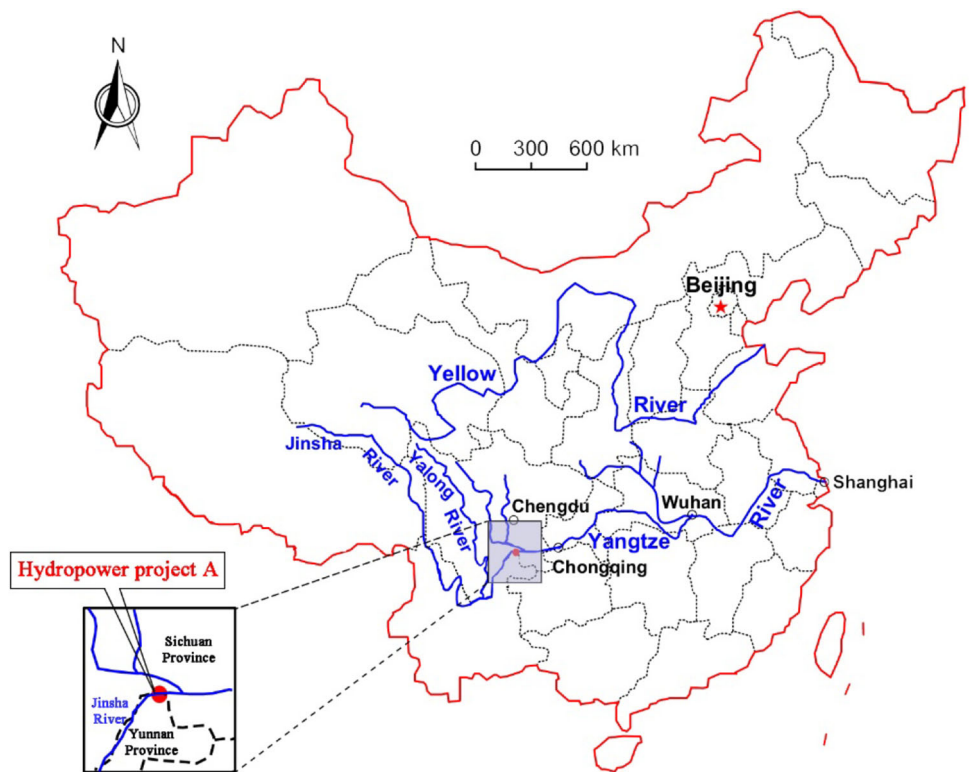
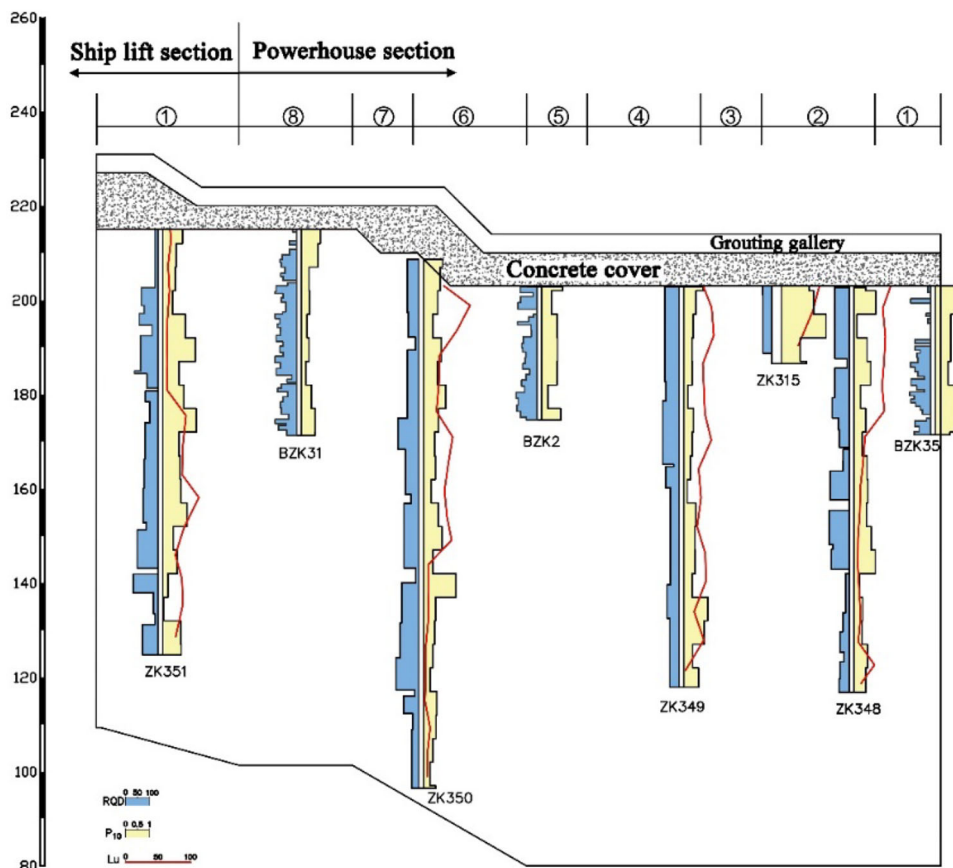


**Fig. 13** Arrangement of grouting curtains



**Fig. 14** Borehole WPTs and coring results from the study region before grouting



**Data collection and analysis**

*Geological properties before grouting*

Before the construction of the grouting curtain, a number of exploratory holes were drilled and cored, and WPTs were carried out to investigate the permeability and fracture properties of the rock mass in the grouting curtain region (the study region shown in Fig. 13). The results, plotted in Fig. 14, show that the distributions of LU values,  $P_{10}$ , and RQD are largely uniform and do not show obvious changes with depth.

This paper uses geostatistical methods to estimate the geological properties of permeability, fracture intensity, and the RQD of the rock mass before grouting for the whole area, including verification holes or points of concern based on the sample point data shown in Fig. 14. First, it is necessary to determine the desired SV functions and Kriging maps in order to obtain the distributions of variables. Investigation of the distribution of variables at the given points is carried out by determining the experimental SV function and then fitting a theoretical model, which is presented in Fig. 15. After the determination of SV functions, the OK method is used for pointwise estimation of the variables. The distributions within the study region are

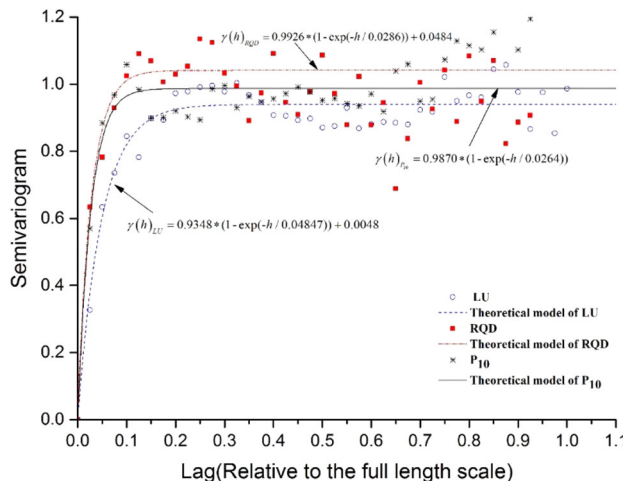


**Fig. 15** SV functions of the ReVs: **a** distribution of LU value, **b** distribution of  $P_{10}$ , **c** distribution of RQD

given in Fig. 16 for the LU values (a),  $P_{10}$  (b), and RQD (c).

*Grouting influence radius*

To estimate the grouting influence radius, seven pairs of grouting boreholes, two primary boreholes separated by

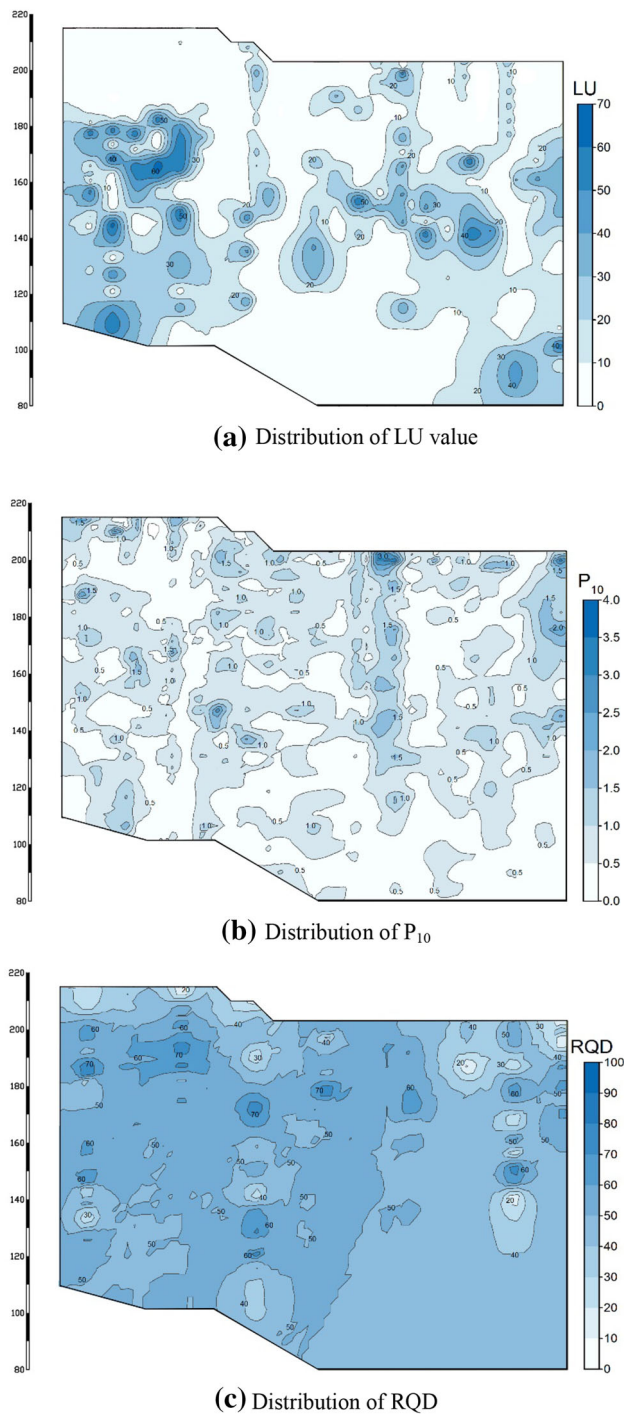


**Fig. 16** Distribution of ReVs in the study area

8 m, and seven pairs of grouting boreholes, one primary and one secondary borehole separated by 4 m, are analyzed. These pairs of grouting boreholes meet the conditions of the proposed estimation method: one is analyzed first, and the other next to it is analyzed later. The ratio of cement takes and ratio of LU values of the neighboring

grouting boreholes are shown in Fig. 17. For example, it can be seen that the cement take and LU values of grouting borehole ZC8-SM-3-12 are 92 and 78% of grouting borehole ZC8-SM-3-08, respectively.

The average ratio of cement takes and ratio of LU values of paired primary boreholes are 0.84 and 0.70, showing that the penetration distance in the fractures is more than half the distance between the boreholes and that existing boreholes influence later boreholes. However, since the average ratio values are not very small, the grouting influence radius should not span the distance between the boreholes. The average ratio of cement takes and the average ratio of LU values for primary and secondary boreholes are 0.16 and 0.22, showing that existing boreholes have strong effects on later boreholes. Since they are small enough, the grouting influence radius should equal or even exceed the distance between the boreholes. Therefore, it can be concluded that the grouting influence radius ranges from the distance between primary and secondary boreholes to the distance between primary boreholes. Here, based on the average ratio of cement takes from pairs of primary boreholes, the grouting influence radius can be calculated using Eqs. 22 and 24, as well as Fig. 7. As the average  $R_{N-P}$  is 0.84, the  $I/D$  value is 0.68. Therefore, the grouting influence radius is 5.44 m when the distance between two primary grouting boreholes is 8 m.

#### *Curtain grouting data*

The ANFIS-based model proposed in this paper was trained and tested with a data set of 740 results from eight exploratory boreholes, 268 grouting boreholes, and 38 verification holes from nine grouting units at the dam site. The influence parameters are obtained before and during the grouting process. These parameters include fracture intensity, the LU value, and RQD before grouting and are estimated using the OK method based on information from exploratory boreholes. Since the grouting influence radius has been obtained beforehand, the effective grouting pressure ( $P_{GE}$ ), effective grouting time ( $T_E$ ), effective grout volume ( $V_{GE}$ ), and effective cement take ( $CT_E$ ) are calculated using the improved IDW method based on grouting operation data gathered during the grouting process. The evaluation indicators of curtain grouting efficiency associated with each sample were obtained from drilling and coring of verification holes, as well as WPTs, borehole television imaging, and estimating the LU value, RQD, and FFR. Summary statistics for the input and output variables are shown in Table 1. Additionally, a list of sample data for training the ANFIS-based model is given in Table 2.

**Fig. 17** Ratio of cement takes and ratio of LU values of pairs of neighboring grouting boreholes

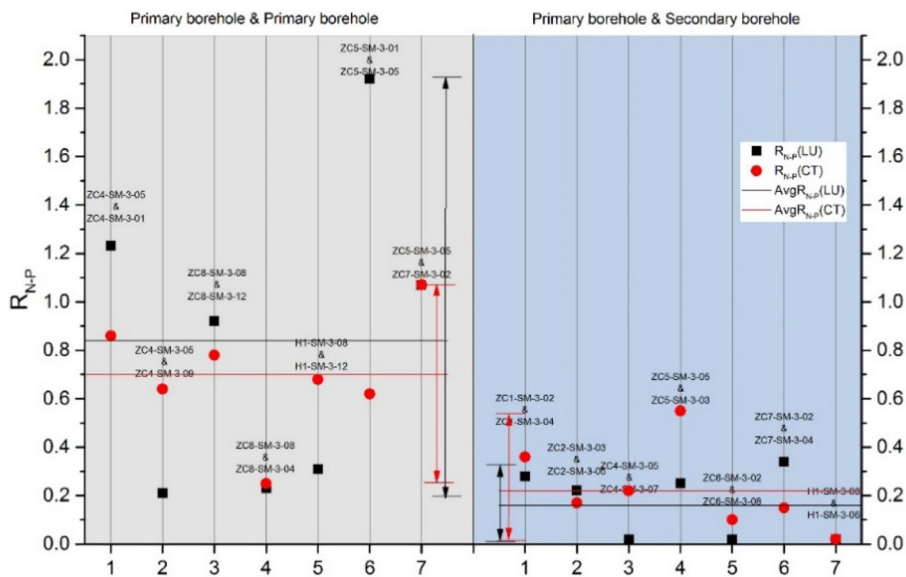


**Table 1** Summary of input and output variables used for prediction of grouting efficiency

Category	Parameter	Symbol	Obtained from	Range	Mean	SD
Input	Depth of the tested interval (m)	H	Verification holes	84–213	158	35
	Fracture intensity (/m)	$P_{10}$	Exploratory boreholes	0.0–5.0	0.6	0.6
	Permeability before grouting (Lu)	$LU_B$		3.24–27.86	14.93	5.13
	RQD before grouting (%)	$RQD_B$		0–100	48	9
	Effective grouting pressure (MPa/m)	$P_{GE}$	Grouting boreholes	6.83–19.80	14.98	2.47
	Effective grouting time (min/m)	$T_E$		72.7–508.3	183.0	65.4
	Effective grout volume (L/m)	$V_{GE}$		40.6–2946.3	887.6	588.4
	Effective cement take ( $kg/m^2$ )	$CT_E$		0.69–2847.4	505.4	484.4
Output	Permeability after grouting (Lu)	$LU_A$	Verification holes	0.03–1.48	0.59	0.26
	RQD after grouting (%)	$RQD_A$		0–100	61	22
	FFR value (%)	FFR		0–100	51	42

**Prediction of curtain grouting efficiency using ANFIS-based models and multiple quality indicators**

*Training and optimization of ANFIS-based models*

In this paper, ANFIS-based models that predict curtain grouting efficiency are proposed to help solve the problem of predicting grouting results. Three ANFIS-based models, including prediction models for permeability, RQD, and FFR, were designed using the Matlab neural network toolbox in this paper and are shown in Fig. 10. Six hundred and seventy observations randomly selected from the data set are used for training, and the remaining data (70 observations) are used for testing. The performance of the ANFIS-based models depends on the system structure. In this study, many attempts have been made to choose the

optimal ANFIS structure by changing the training options in the ANFIS algorithm.

To determine the number of fuzzy rules, many models with different numbers of fuzzy rules (e.g., two and three) were employed separately for the LU value, RQD, and FFR variables. Eventually, it was found that input parameters with three fuzzy rules perform better than the other ANFIS models for predicting the LU value, RQD, and FFR. As the system has eight parameters and each has three subclasses, the number of if–then rules used in predicting the LU value, RQD, and FFR is then 6561 ( $3^8$ ). For the fuzzy MFs, this paper selects the generalized bell membership function (gbellmf) for use as the input MF. The output MF is linear. Table 3 shows the types of the parameters and their values used in the ANFIS models.

**Table 2** Sample of data set used for prediction of grouting efficiency

Nos.	Input parameters								Output parameters		
	$H$ (m)	$P_{10}$ (/m)	$LU_B$ (Lu)	$RQD_B$ (%)	$P_{GE}$ (MPa/m)	$T_E$ (min/m <sup>2</sup> )	$V_{GE}$ (L/m <sup>2</sup> )	$CT_E$ (kg/m <sup>2</sup> )	$LU_A$ (Lu)	$RQD_A$ (%)	FFR (%)
1	202	1.0	21.69	18	10.3	219.6	149.6	0.7	0.46	33	50
2	201	4.0	21.54	27	11.6	483.0	628.9	105.3	0.49	43	25
3	199	2.5	21.00	24	12.6	271.0	309.8	30.3	0.19	80	0
4	196	1.8	20.89	18	13.6	130.3	496.4	235.6	0.12	46	33
5	191	1.0	19.87	41	14.9	187.3	598.9	274.3	0.21	59	80
6	186	1.4	18.41	60	16.2	149.6	530.1	211.5	0.60	71	71
7	181	0.8	16.84	60	17.4	149.1	934.6	492.0	0.30	72	25
8	176	2.4	16.21	46	19.2	190.2	825.7	420.1	0.44	49	83
9	171	1.6	15.24	60	19.2	190.2	825.7	420.1	0.48	71	25
10	166	1.0	15.49	63	19.4	210.4	708.0	304.4	0.65	64	20

**Table 3** Parameters used in ANFIS models

ANFIS parameters	Value	ANFIS parameters	Value
Type	Sugeno	Number of nodes	13,181
Number of inputs	8	Number of linear parameters	59,049
Number of outputs	3 (1 at a time)	Number of nonlinear parameters	72
Number of input membership functions	$3 \times 8$	Total number of parameters	59,121
Input membership function	Gbellmf	Number of training data pairs	670
Output membership function	Linear	Number of testing data pairs	70
Number of fuzzy rules	6561	Number of epochs	200

### Prediction results of ANFIS-based models

Graphs comparing the predicted grouting efficiency of the LU value, RQD, and FFR using the ANFIS-based models to the measured values in the testing data set are shown in Figs. 18 and 23. The average deviations between the predicted and measured values are 4, 0.05, and 5 for the LU value, RQD, and FFR, with average absolute deviations of 8, 7, and 8%, respectively. Figure 18 also identifies areas corresponding to an absolute deviation of 5, 10, and 20%. Most of the predicted values are in the 10% area, and a few fall within 20%. These results demonstrate the ability of the ANFIS-based models to predict the LU value, RQD, and FFR after grouting with a high degree of accuracy. As shown in Fig. 18, the ANFIS-based models encountered some difficulties in learning the complex relationships between the LU value, RQD, and FFR of some samples and their contributing factors, where the predicted value deviated from the measured value by 20% or more.

### Evaluation of grouting efficiency based on the predictions of ANFIS-based models

To assess curtain grouting quality, the spatial distributions of the LU value, RQD, and FFR after grouting are predicted by the proposed ANFIS-based method. These distributions cannot be obtained using traditional in situ tests based on samples from drill holes.

Figure 19 shows the distributions of the LU value, RQD, and FFR in Unit 1 of the powerhouse section on the curtain grouting line after grouting. From the resulting contour map, it can be seen that the LU value is mainly concentrated in the range 0.4–0.6 Lu, which is less than the design standard of 1 Lu. However, there is a small area with permeability greater than 1 Lu in the lower left corner of the figure, which the WPTs did not detect. On the whole, the distribution is relatively uniform, without dramatic changes or abnormal areas. The same situation also applies to the RQD indicator: the values are mainly concentrated in the range 40–80 without abnormal areas. The FFR values

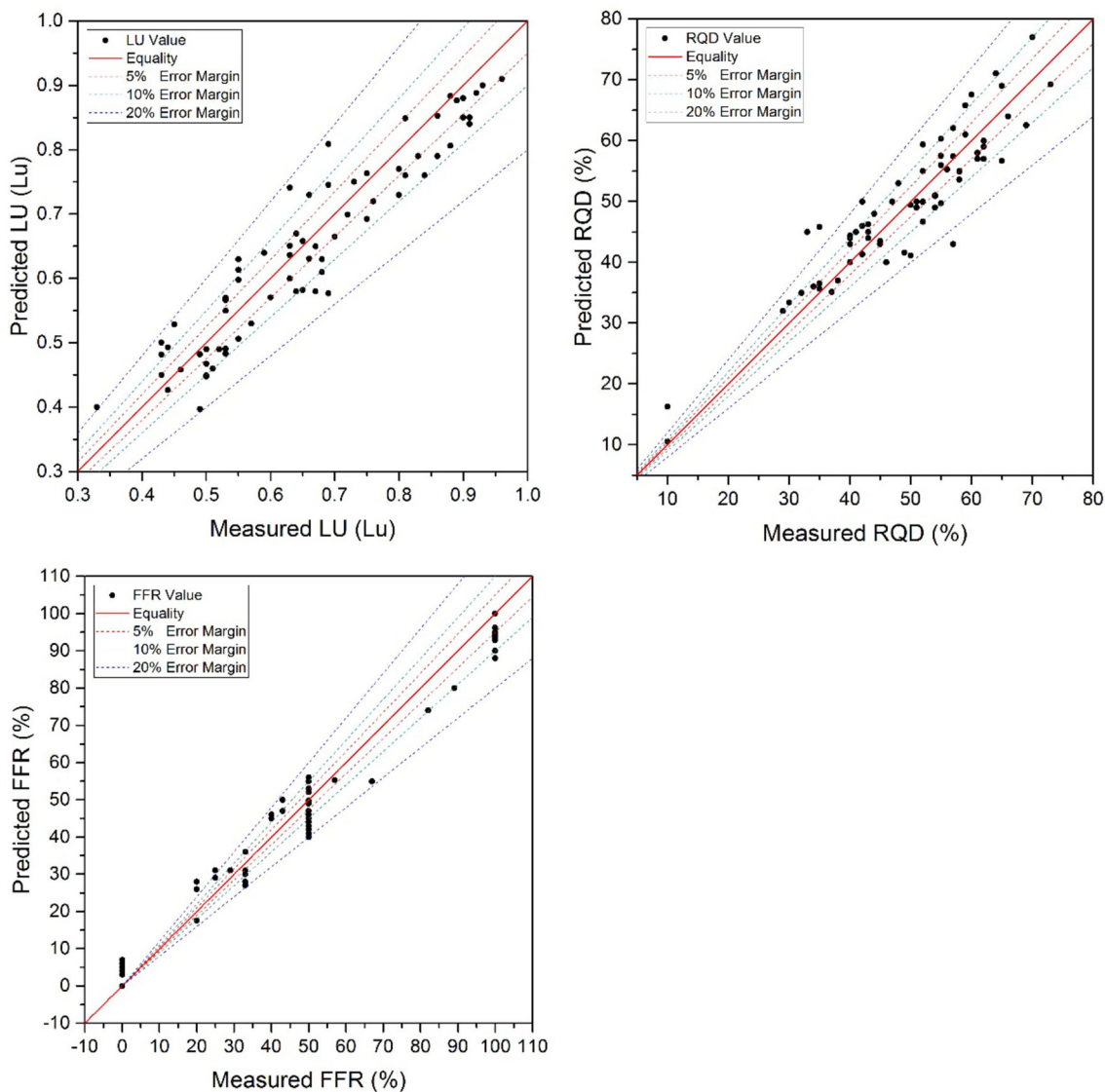


**Fig. 18** Predicted values of LU, RQD, and FFR by the ANFIS-based models against the measured values

are mainly concentrated in the range of 40–80, showing that the filling effect is good, except in the small region in the upper right, where the FFR value is less than 20%.

Additionally, from the distribution curves of Lu plotted in Fig. 20, it is clear that after improvement by grouting the LU values in study zone are reduced. After grouting was performed, more than 95% of the grouted area has a permeability less than 1 Lu, while the value before grouting is less than 10%. In addition, its middle value  $LU_{50}$  diminishes from 10.2 to 0.2 Lu. Moreover, the average RQD increases to 61 after injection. This increase corresponds to 50% of the value before grouting, which is 42.

In a previous study reported by Fan et al. (2016), standard values for efficiency-level classifications of the evaluation indicators were proposed, as shown in Table 4.

The frequency of each indicator in each classification can be calculated based on the efficiency-level classification and values of the indicators, shown in Fig. 21. On the basis of this efficiency-level classification, LU values of 0.8% are good, 96.7% fine, 2.5% ordinary, 0% poor, and 0% bad. RQD values of 6.6% are good, 15.6% fine, 54.9% ordinary, 22.1% poor, and 0.8% bad. FFR values of 13.1% are good, 5.8% fine, 30.3% ordinary, 26.2% poor, and 24.6% bad.

It can be seen from the above results that curtain grouting has proven quite effective in reducing the permeability and improving the integrity and watertightness of the rock mass. It reveals that cement grouting has penetrated into the main rock fractures and filled the voids, leading to a significant improvement in the dam foundation.

**Fig. 19** The distributions of LU, RQD, and FFR in Unit 1

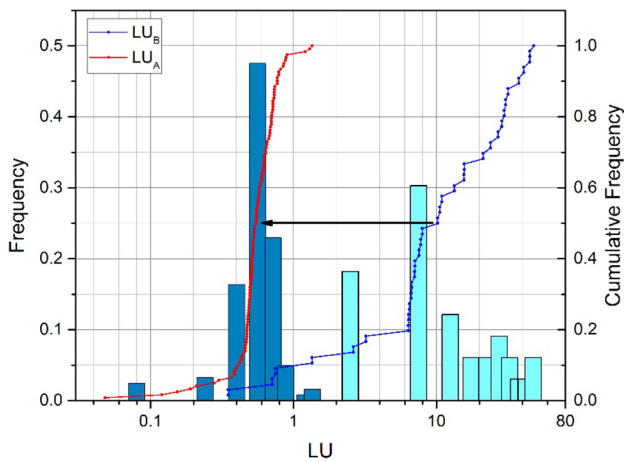
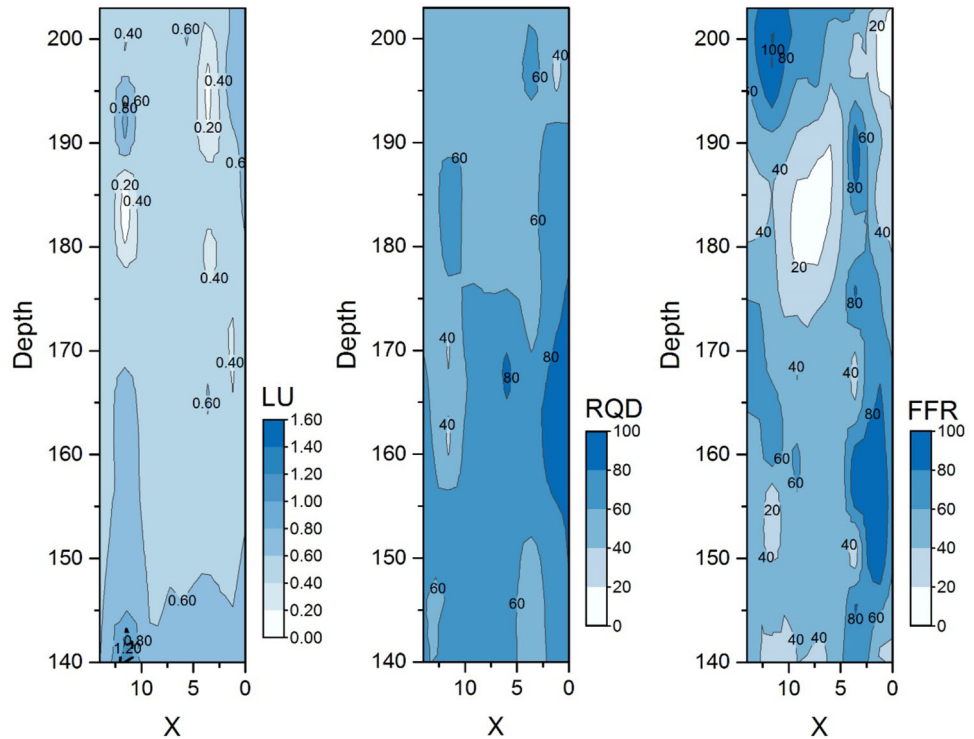


**Fig. 20** Histograms and cumulative distribution functions of Lu before and after grouting

**Discussion**

This paper presents a method for estimating the grouting influence radius based on the cement take of grouting boreholes. The grouting influence radius helps to determine

which grouting boreholes are within the functioning range. It provides an empirical standard to determine whether a grout hole take effect on improvement of a certain position. Obviously, it plays a certain role in the estimate of grouting effect. We have compared the results of calculating the grouting influence radius with some previous studies that estimated grout penetration, as presented in Fig. 22. The red line represents grouting influence radius estimated by the proposed method, and the blue points are grouting penetration depth calculated by reference to previous studies. According to the results, the grout penetration distances estimated by different calculation models varied over a wide range, of which the maximum value of 77.4 m was reported by Funehag and Fransson (2006) and Funehag and Gustafson (2008a, b), while the minimum value of 0.36 m was reported by Hu (2005). Since the penetration distances in these studies are mainly obtained by theoretical calculation, with some simplification and idealization, there are differences between field results and the theoretical calculations. The estimation formula of grouting influence radius proposed in this paper is different from those used in previous studies, in that it is based on the

**Table 4** Efficiency-level classification standard for the evaluation indicators

Efficiency level	I (good)	II (fine)	III (ordinary)	IV (poor)	V (bad)
LU (Lu)	<0.1	0.1–1	1–1.5	1.5–2	>2
RQD (%)	90–100	75–90	50–75	25–50	<25
FFR (%)	90–100	75–90	50–75	25–50	<25

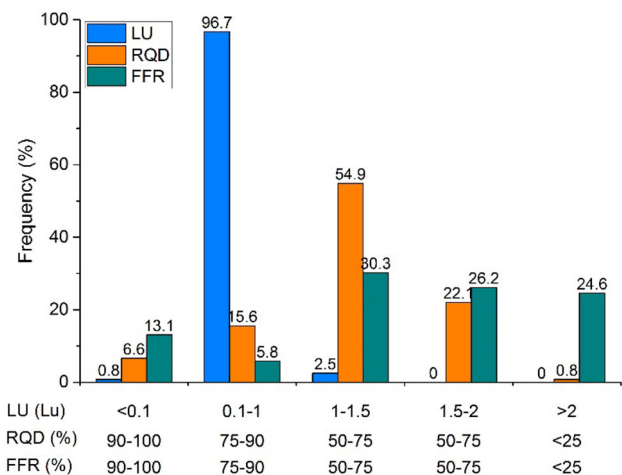


**Fig. 21** Frequency distribution of the indicators in each efficiency-level classification

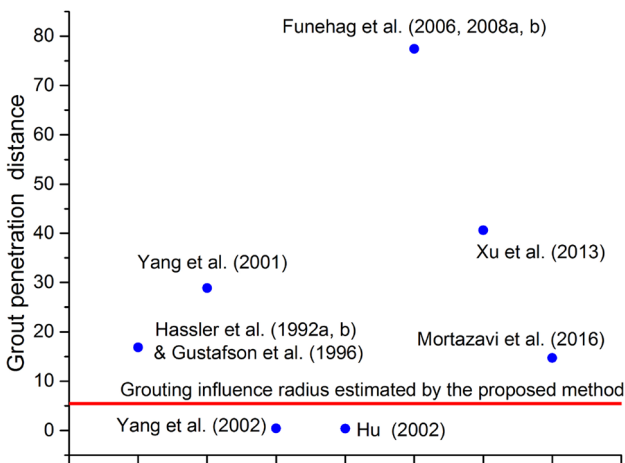


**Fig. 22** Grout penetration as estimated by different studies

cement take of grouting boreholes. Therefore, it provides a more accurate assessment of the grouting influence radius. Because of the complex characteristics of rock mass and the hidden diffusion grouting process, it is difficult to monitor the diffusion process during the construction. Some in-field tests, such as WPTs, acoustic velocity tests, and some geotechnical and geophysical tests, show effectiveness in evaluating the grouting performance of reducing permeability, and improving strength of rock foundations. However, the grouting penetration distance cannot be accurately evaluated by these tests directly. Drilling verification holes or excavation is commonly used to verify the result of fractures filled by grout and the penetration length by visual observation (Funehag and Fransson 2006; Huang et al. 2012). However, drilling many verification holes or excavation would damage the integrity of the rock foundation, and interfere the grouting construction. Therefore, it was very difficult to make a field test

validation. If conditions permit, appropriate field test validation will be carried on in a future work.

To illustrate the effectiveness of the method presented in this paper, we compare the calculation results of LU, RQD, and FFR estimated by the proposed method with the field data obtained from the in situ tests for two verification holes. Figure 23 shows two verification holes selected from Unit 1 (Fig. 14): the verification hole I (ZC1-SM-ZJ-1) on the left side and verification hole II (ZC1-SM-ZJ-2) on the right side. These two boreholes are drilled from an elevation of 203 m to a depth of 70 m. The LU, RQD, and FFR values of verification holes were obtained from drilling and coring, as well as WPTs, borehole television imaging, and estimating. The calculation results of LU, RQD, and FFR were estimated by the proposed method. The LU values are shown in ascending order from left to right on the lower horizontal axis and the RQD and FFR values are presented in ascending order from left to right on the upper horizontal axis in Fig. 23. The field data of LU, RQD, and FFR values are drawn by solid line with filled symbol, and the calculation results of LU, RQD, and FFR values are drawn by a dashed line with unfilled symbols. According to the field data of the two verification holes shown in Fig. 23, it can be seen that the LU values are mainly concentrated in range 0–1 Lu, which is less than the design standard of 1 Lu. However, there is one segment with permeability greater than 1 Lu at 60–65 m of the verification hole I. The same situation also applies to the RQD indicator: the values are mainly concentrated in the range 20–80. The FFR values show a large variation range; however, most of the values are greater than 20, showing that the main fractures have been filled. The frequency of each indicator in each efficiency-level classification were calculated based on Table 4, shown in Fig. 24. On the basis of this efficiency-level classification, LU values of 3.1% are good, 93.8% fine, 3.1% ordinary, 0% poor, and 0% bad. RQD values of 0% are good, 3.1% fine, 31.3% ordinary, 53.1% poor, and 12.5% bad. FFR values of 18.8% are good, 12.5% fine, 18.8% ordinary, 28.1% poor, and 21.9% bad. It can be seen from the field results that the curtain grouting has proved quite effective in reducing the permeability. The cement grouting has penetrated into the main rock fractures and filled the voids, leading to a significant improvement in the dam foundation.

It shows the comparison between the calculation results and field data of the LU, RQD, and FFR values in Figs. 23 and 24. According to Fig. 23, the calculation results of LU, RQD, and FFR estimated by the proposed method are in good agreement with the field data. The average deviations between the calculation and field data values are 0.1, 8, and 14 for the LU value, RQD, and FFR, with a high degree of accuracy. As can be seen from Fig. 24, the frequency of each indicator in each efficiency-level classification of

**Fig. 23** Comparison of calculation results of LU, RQD, and FFR with the field data for two verification holes

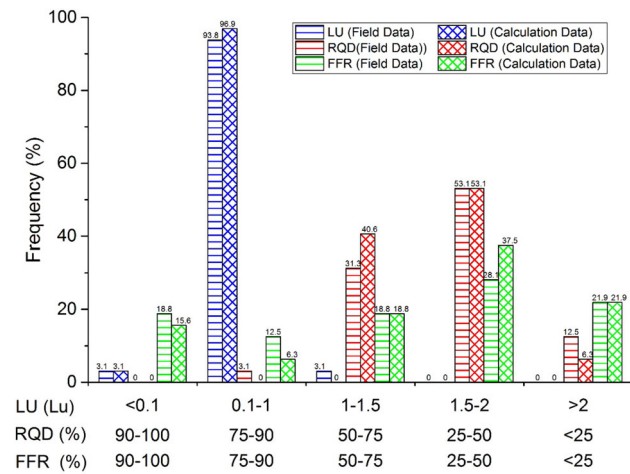
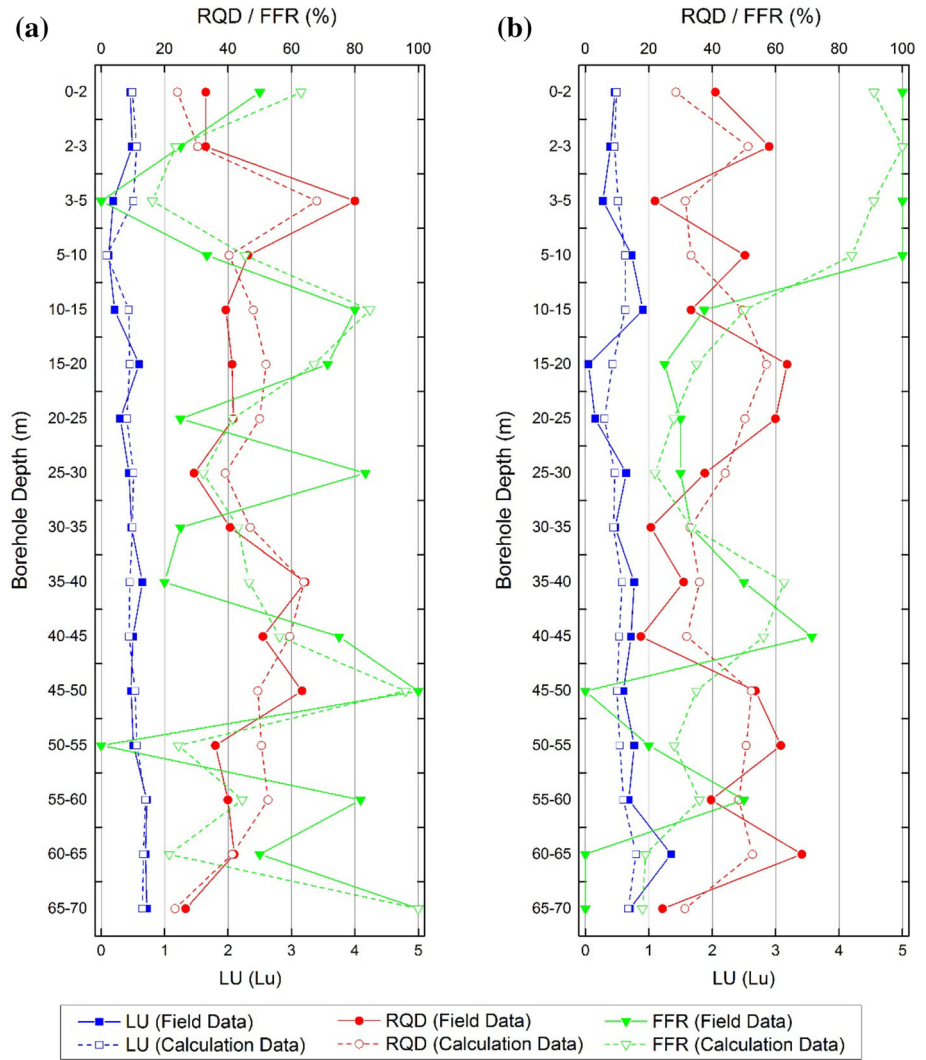


**Fig. 24** Comparison of frequency distribution of the LU, RQD, and FFR in each efficiency-level classification of calculation results with the field data for two verification holes

calculation results of LU, RQD, and FFR is in accordance with the field results.

Additionally, this study has compared the prediction performance of ANFIS-based models with the artificial neural network (ANN) and multiple linear regression (MLR) methods. Using the same training and testing data sets, a three-layer (8-15-3) BP neural-network model is designed, trained, and tested, after some optimization, using the Matlab neural network toolbox. Additionally, three simple linear regression equations are obtained by using the Matlab toolbox for regression analysis, that expresses the relationships between the LU value, RQD, and FFR and the parameters described by Eqs. 42, 43, and 44.

$$LU_A = 1.505 - 0.004H + 0.008P_{10} - 0.005 \times LU_B - 0.022 \times P_{GE} \tag{42}$$



$$\begin{aligned}
 RQD_A = & 9.782 - 0.057 \times H + 0.531 \times RQD_B \\
 & - 2.703 \times P_{10} + 0.64 \times LU_B \\
 & - 0.001 \times V_{GE} + 0.004 \times CT_E - 0.012 \\
 & \times T_E + 1.158 \times P_{GE}
 \end{aligned} \tag{43}$$

$$\begin{aligned}
 FFR = & 11.835 + 0.359 \times H - 0.087 \times RQD_B \\
 & - 19.352 \times P_{10} - 0.282 \times LU_B - 0.002 \\
 & \times V_{GE} + 0.026 \times T_E - 0.026 \times P_{GE}
 \end{aligned} \tag{44}$$

For the performance prediction of curtain grouting efficiency, the LU, RQD, and FFR values are predicted by using presently ANFIS models, ANN, and MLR, and the obtained results are given in Fig. 25. Figure 25 plots the predicted LU, RQD, and FFR values, as well as the prediction error of each method, versus the field measured values, for the ANFIS, ANN, and MLR models. To check and compare the prediction performances of the ANFIS, ANN, and MLR-based models, the root mean square error

RMSE (Eq. 45), the coefficient of determination  $R^2$  (Eq. 46) and the variance accounted for VAF (Eq. 47) indexes are used:

$$RMSE = \sqrt{\frac{\sum_{i=1}^N (O_M - O_P)^2}{N}} \tag{45}$$

$$R^2 = 1 - \frac{\sum_{i=1}^N (O_M - O_P)^2}{\sum_{i=1}^N (O_M - \bar{O}_M)^2} \tag{46}$$

$$VAF = \left[ 1 - \frac{\text{var}(O_M - O_P)}{\text{var}(O_M)} \right] \times 100 \tag{47}$$

where  $O_M$ ,  $O_P$ , and  $\bar{O}_M$  are the measured, predicted and mean  $O_M$  values, respectively, and  $N$  is the total number of observations.

Table 5 shows the performance of the three models as measured using RMSE,  $R^2$  and VAF in the testing process. The obtained results indicate that the ANFIS-based models

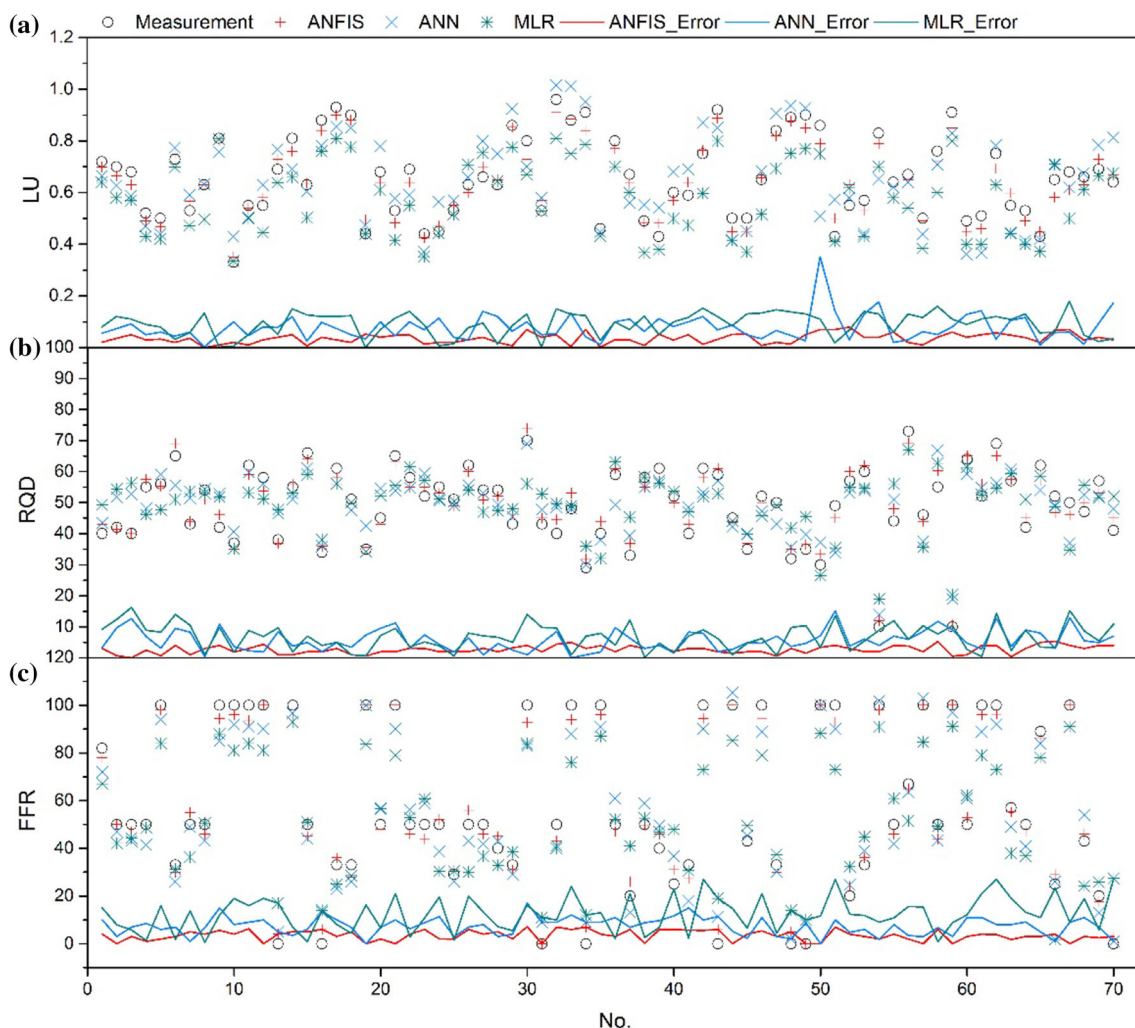


**Fig. 25** Comparison of predicted results with actual measured values for LU, RQD, and FFR based on the ANFIS, ANN, and MLR-based models

**Table 5** Values of RMSE,  $R^2$  and VAF for each model

Model	LU			RQD			FFR		
	RMSE	$R^2$	VAF	RMSE	$R^2$	VAF	RMSE	$R^2$	VAF
ANFIS	4.82	0.848	84.8	0.05	0.883	88.9	5.59	0.973	97.6
ANN	6.65	0.710	80.0	0.09	0.637	63.9	8.23	0.942	94.7
MLR	7.95	0.586	58.6	0.10	0.566	84.2	14.4	0.820	84.0

perform best (that is, they have the smallest RMSE values and the highest  $R^2$  and VAF values for LU, RQD, and FFR), followed by the ANN-based model and the MLR model. Because of the complicated geological properties of the dam foundation and the many uncertainties in the grouting operation, it is more suitable to use nonlinear prediction methods to solve the problem of predicting the result of grouting. It is difficult to obtain an exact relationship between the variables, and that is why the prediction performances of the two AI models are higher than those of MLR. ANFIS is the result of ANN and FL in combination. Combining these two intelligent approaches, a good result is achieved in both quality and quantity. Therefore, the results showed that the ANFIS model performed slightly better than the ANN-based one. Generally, the results reveal that ANFIS-based models can be introduced as a powerful tool for prediction of grouting efficiency in terms of the LU value, RQD, and FFR in curtain grouting operations.

## Conclusion

In this study, prediction models based on ANFIS methods are proposed to evaluate curtain grouting efficiency. Attempts have been made to further understand the relationship between grouting efficiency and influencing factors. Geological factors (including permeability, fracture intensity, and RQD before grouting), grouting operation factors (including grouting pressure, grouting time, grout volume, and the cement take during the grouting process), and the depth of the tested interval are considered to be the critical factors that can greatly influence the efficiency of curtain grouting and are, therefore, selected as input parameters. The grouting efficiency evaluation indicators (the LU value, RQD, and FFR after grouting) are selected as output parameters and are integrated into a comprehensive evaluation.

In this paper, to determine the influence range of grouting boreholes, a formula for estimating the radius of influence of grouting boreholes is proposed. The paper uses the OK method to calculate the values of geological factors. To reflect better the influence of the grouting boreholes' position on the effects of grouting, this study proposes new parameters to describe grouting operation

factors. These parameters include the effective grouting pressure ( $P_{GE}$ ), effective grouting time ( $T_E$ ), effective grout volume ( $V_{GE}$ ), and effective cement take ( $CT_E$ ), which are calculated using an improved IDW method.

As a case study, we apply ANFIS-based models to predict the results of grouting and to evaluate the efficiency of curtain grouting of hydropower project A in the southwestern part of China. As a result of this study, the following conclusions can be drawn:

1. The improvement in the properties of dam foundations, including the LU value, RQD, and FFR, after curtain grouting can be predicted quickly and accurately using prediction models based on ANFIS.
2. The effects of grouting at a certain location is influenced by the grouting boreholes within the grout penetration depth. The method of estimating the radius of grouting influence proposed in this paper helps to determine which grouting boreholes are within the functioning range.
3. Compared with traditional in situ tests, the proposed method has many advantages. First and most importantly, it can evaluate grouting effect in advance, while traditional methods only evaluate the efficiency after all field verification tests have been completed. It is highly time and labor-saving and is a nondestructive evaluation method that does not require drilling verification holes. Furthermore, it can predict the effects of grouting over an entire area, removing an important limitation of sample tests. Additionally, the combination of direct test methods and the prediction method should be recommended for evaluating the effects of grouting. This combination can decrease the need for in situ tests and increase the reliability of grouting effect evaluation.

However, because of the complexity of geological conditions and engineering operations, as well as the uncertain relationships between evaluation indicators and the factors that influence them, making predictions of grouting efficiency is very difficult. Therefore, constant optimization of the prediction model should be made to improve the prediction effectiveness. In addition, the theory of grout penetration in fracture rock mass needs additional research to further understand the mechanisms of grouting and sealing.

**Acknowledgements** This research is supported by the Natural Science Foundation of China (Grant Nos. 51439005 and 51339003) and the National Basic Research Program of China 973 Program (Grant No. 2013CB035904).

## References

- Ahmed S, De Marsily G (1987) Comparison of geostatistical methods for estimating transmissivity using data on transmissivity and specific capacity. *Water Resour Res* 23(9):1717–1737
- Akhondi M, Mohammadi Z (2014) Preliminary analysis of spatial development of karst using a geostatistical simulation approach. *B Eng Geol Environ* 73(4):1037–1047. doi:10.1007/s10064-014-0599-3
- Amadei B, Savage WZ (2001) An analytical solution for transient flow of Bingham viscoplastic materials in rock fractures. *Int J Rock Mech Min* 38(2):285–296. doi:10.1016/S1365-1609(00)00080-0
- Azimian A, Ajalloeian R (2015) Permeability and groutability appraisal of the Nargesi dam site in Iran based on the secondary permeability index, joint hydraulic aperture and Lugeon tests. *B Eng Geol Environ* 74(3):845–859. doi:10.1007/s10064-014-0675-8
- Bryson L S, Ortiz R, Leandre J (2014) Effects of a grout curtain on hydraulic and electrical conductivity in a laboratory-scale seepage model[C]. In: 2014 congress on geo-characterization and modeling for sustainability. Geo-Congress 2014, Atlanta, United States pp 3233–3242
- Carter TG, Dershowitz W, Shuttle DA, Jefferies M (2012) Improved methods of design for grouting fractured rock. In: Proceedings of the 4th international conference on grouting and deep mixing, pp 1472–1483
- Chen M, Lu W, Zhang W, Yan P, Zhou C (2015) An analysis of consolidation grouting effect of bedrock based on its acoustic velocity increase. *Rock Mech Rock Eng* 48(3):1259–1274. doi:10.1007/s00603-014-0624-7
- Cheng M, Hoang N (2014) Groutability prediction of microfine cement based soil improvement using evolutionary LS-SVM inference model. *J Civ Eng Manag* 20(6):839–848
- Chiles JP (1988) Fractal and geostatistical methods for modeling of a fracture network. *Math Geol* 20(6):631–654
- Deere DU (1962) Technical description of rock cores for engineering purposes. University of Illinois, Illinois
- Deere DU (1968) Chapter 1: geological considerations. In: Stagg KG, Zienkiewicz OC (eds) *Rock mechanics in engineering practice*, Wiley, London pp 1–20.
- Ehsanzadeh B, Ahangari K (2014) A novel approach in estimation of the soilcrete column's diameter and optimization of the high pressure jet grouting using adaptive neuro fuzzy inference system (ANFIS). *Open J Geol* 04(08):386–398. doi:10.4236/ojg.2014.48030
- Eriksson M, Friedrich M, Vorschulze C (2004) Variations in the rheology and penetrability of cement-based grouts—an experimental study. *Cem Concr Res* 34(7):1111–1119
- Ewert F (1994) Evaluation and interpretation of water pressure tests. *Grouting in the ground*. Thomas Telford, London, pp 141–162
- Ewert F (1997) Permeability, groutability and grouting of rocks related to dam sites part 3. *Dam Eng* 8:215–248
- Fan G, Zhong D, Yan F, Yue P (2016) A hybrid fuzzy evaluation method for curtain grouting efficiency assessment based on an AHP method extended by D numbers. *Expert Syst Appl* 44:289–303. doi:10.1016/j.eswa.2015.09.006
- Ferrari F, Apuani T, Giani GP (2014) Rock mass rating spatial estimation by geostatistical analysis. *Int J Rock Mech Min* 70:162–176. doi:10.1016/j.ijrmm.2014.04.016
- Fransson Å (2001) Characterisation of a fractured rock mass for a grouting field test. *Tunn Undergr Sp Tech* 16(4):331–339
- Funehag J, Fransson Å (2006) Sealing narrow fractures with a Newtonian fluid: model prediction for grouting verified by field study. *Tunn Undergr Sp Tech* 21(5):492–498. doi:10.1016/j.tust.2005.08.010
- Funehag J, Gustafson G (2008a) Design of grouting with silica sol in hard rock—new methods for calculation of penetration length. Part I. *Tunn Undergr Sp Tech* 23(1):1–8. doi:10.1016/j.tust.2006.12.005
- Funehag J, Gustafson G (2008b) Design of grouting with silica sol in hard rock—new design criteria tested in the field. Part II. *Tunn Undergr Sp Tech* 23(1):9–17. doi:10.1016/j.tust.2006.12.004
- Guo X, Meng S (2011) Intelligent prediction on toe- slab foundation grouting of high faced rockfill dam based on LIBSVM. *Yangtze River* 42(01):33–36 (in Chinese)
- Gustafson G (2012) *Hydrogeology for rock engineers*. BeFo Rock Eng Res Found, Stockholm
- Gustafson G, Stille H (1996) Prediction of groutability from grout properties and hydrogeological data. *Tunn Undergr Sp Tech* 11(3):325–332
- Håkansson U (1993) *Rheology of fresh cement based grouts*. PhD Thesis, Royal Institute of Technology
- Hassanlourad M, Vosoughi M, Sarrafi A (2014) Predicting the grouting ability of sandy soils by artificial neural networks based on experimental tests. *Civil Eng Infrastruct J* 47(2):239–253
- Hässler L, Håkansson U, Stille H (1992a) Computer-simulated flow of grouts in jointed rock. *Tunn Undergr Sp Tech* 7(4):441–446
- Hässler L, Håkansson U, Stille H (1992b) Classification of jointed rock with emphasis on grouting. *Tunn Undergr Sp Tech* 7(4):447–452
- Hu J (2005) *The research for the state grouting experiment in cracked rock mass*. Central South University, Changsha (in Chinese)
- Huang XG, Yang XL, Fang YZ (2012) Study on grouting effect evaluation of F4 weathered slot in Xiamen Xiang'an submarine tunnel. *Appl Mech Mater* 256:1217–1220
- Huo J, Song H, Luo L (2015) Investigation of groundwater chemistry at a dam site during its construction: a case study of Xiangjiaba Dam, China. *Environ Earth Sci* 74(3):2451–2461. doi:10.1007/s12665-015-4261-6
- Jahed Armaghani D, Tonnizam Mohamad E, Momeni E, Narayanasamy MS, Mohd Amin MF (2015) An adaptive neuro-fuzzy inference system for predicting unconfined compressive strength and Young's modulus: a study on Main Range granite. *B Eng Geol Environ* 74(4):1301–1319. doi:10.1007/s10064-014-0687-4
- Jaksa MB, Maier HR, Shahin MA (2008) Future challenges for artificial neural network modelling in geotechnical engineering. In: *The 12th international conference of international association for computer methods and advances in geomechanics (IAC-MAG)*, Geo, India
- Jang J (1993) ANFIS: adaptive-network-based fuzzy inference system. *IEEE Trans Syst Man Cybern* 23(3):665–685
- Kayabasi A, Yesiloglu-Gultekin N, Gokceoglu C (2015) Use of non-linear prediction tools to assess rock mass permeability using various discontinuity parameters. *Eng Geol* 185:1–9. doi:10.1016/j.enggeo.2014.12.007
- Kikuchi K, Igari T, Mito Y, Utsuki S (1997) In situ experimental studies on improvement of rock masses by grouting treatment. *Int J Rock Mech Min* 34(3):131–138
- Kim J, Yoon W (2014) Application of resistivity monitoring to evaluate cement grouting effect in earth filled dam. In: *Proceedings of the international conference on numerical analysis and applied mathematics 2014 (ICNAAM-2014)*, 270005
- Kucuk K, Aksoy CO, Basarir H, Onargan T, Genis M, Ozacar V (2011) Prediction of the performance of impact hammer by

- adaptive neuro-fuzzy inference system modelling. *Tunn Undergr Sp Tech* 26(1):38–45. doi:[10.1016/j.tust.2010.06.011](https://doi.org/10.1016/j.tust.2010.06.011)
- Kvartberg S, Fransson Å (2013) Hydrogeological characterisation and stochastic modelling of a hydraulically conductive fracture system affected by grouting: a case study of horizontal circular drifts. *Tunn Undergr Sp Tech* 38:38–49
- Lei JS, Chen JF, Cao XT, Wang QF (2013) The regression prediction analysis of grouting concretion Stone's strength based on SVR. *Adv Mater Res* 859:171–176. doi:[10.4028/www.scientific.net/AMR.859.171](https://doi.org/10.4028/www.scientific.net/AMR.859.171)
- Li J, Zhao Q, Fu R, Yang Y (2001) The application of artificial neural network in grouting projects. *J Geol Hazards Environ Preserv* 12(03):85–88 (in Chinese)
- Liao K, Fan J, Huang C (2011) An artificial neural network for groutability prediction of permeation grouting with microfine cement grouts. *Comput Geotech* 38(8):978–986. doi:[10.1016/j.compgeo.2011.07.008](https://doi.org/10.1016/j.compgeo.2011.07.008)
- Lin P, Zhu X, Li Q, Liu H, Yu Y (2016) Study on optimal grouting timing for controlling uplift deformation of a super high arch dam. *Rock Mech Rock Eng* 49(1):115–142. doi:[10.1007/s00603-015-0732-z](https://doi.org/10.1007/s00603-015-0732-z)
- Lisa H, Christian B, Åsa F, Gunnar G, Johan F (2012) A hard rock tunnel case study: characterization of the water-bearing fracture system for tunnel grouting. *Tunn Undergr Sp Tech* 30:132–144
- Long J, Billaux DM (1987) From field data to fracture network modeling: an example incorporating spatial structure. *Water Resour Res* 23(7):1201–1216
- Lu GY, Wong DW (2008) An adaptive inverse-distance weighting spatial interpolation technique. *Comput Geosci-UK* 34(9):1044–1055
- Lugeon M (1933) Barrages et geologic methods de recherche terrassement et un permeabilisation. Litrairedes Universite, Paris
- Lynch C, Dodson M, McCartney JS (2012) Grouting verification using 3-d seismic tomography. *Grout Deep Mix* 2012:1506–1515
- Mortazavi A, Maadikhah A (2016) An investigation of the effects of important grouting and rock parameters on the grouting process. *Geomech Geoen* 11:1–17
- Oh H, Pradhan B (2011) Application of a neuro-fuzzy model to landslide-susceptibility mapping for shallow landslides in a tropical hilly area. *Comput Geosci-UK* 37(9):1264–1276. doi:[10.1016/j.cageo.2010.10.012](https://doi.org/10.1016/j.cageo.2010.10.012)
- Ozturk CA, Simdi E (2014) Geostatistical investigation of geotechnical and constructional properties in Kadikoy-Kartal subway, Turkey. *Tunn Undergr Sp Tech* 41:35–45. doi:[10.1016/j.tust.2013.11.002](https://doi.org/10.1016/j.tust.2013.11.002)
- Palmstrom A (2005) Measurements of and correlations between block size and rock quality designation (RQD). *Tunn Undergr Sp Tech* 20(4):362–377
- Rafiee A, Vinches M (2008) Application of geostatistical characteristics of rock mass fracture systems in 3D model generation. *Int J Rock Mech Min* 45(4):644–652
- Razack M, Lasm T (2006) Geostatistical estimation of the transmissivity in a highly fractured metamorphic and crystalline aquifer (Man-Danane Region, Western Ivory Coast). *J Hydrol* 325(1):164–178
- Roman WM, Hockenberry AN, Berezniak JN, Wilson DB, Knight MA (2013) Evaluation of grouting for hydraulic barriers in rock. *Environ Eng Geosci* 19(4):363–375
- Sadeghiyeh SM, Hashemi M, Ajalloeian R (2013) Comparison of permeability and groutability of Ostur Dam site rock mass for grout curtain design. *Rock Mech Rock Eng* 46(2):341–357. doi:[10.1007/s00603-012-0282-6](https://doi.org/10.1007/s00603-012-0282-6)
- Saeidi O, Stille H, Torabi SR (2013) Numerical and analytical analyses of the effects of different joint and grout properties on the rock mass groutability. *Tunn Undergr Sp Tech* 38:11–25. doi:[10.1016/j.tust.2013.05.005](https://doi.org/10.1016/j.tust.2013.05.005)
- Shahin MA, Jaksa MB, Maier HR (2001) Artificial neural network applications in geotechnical engineering. *Aust Geomech* 36(1):49–62
- Shuttle DA, Dershowitz W, Glynn E, Burch S, Novak T (2000) Discrete fracture network analysis of foundation grouting. In: 4th North American rock mechanics symposium
- Singh R, Kainthola A, Singh TN (2012) Estimation of elastic constant of rocks using an ANFIS approach. *Appl Soft Comput* 12(1):40–45. doi:[10.1016/j.asoc.2011.09.010](https://doi.org/10.1016/j.asoc.2011.09.010)
- Snow DT (1968) Rock fracture spacings, openings and porosities. *J Soil Mech Found Div Proc Am Soc Civil Eng* 94:73–91
- Sohrabi-Bidar A, Rastegar-Nia A, Zolfaghari A (2015) Estimation of the grout take using empirical relationships (case study: Bakhtiari dam site). *B Eng Geol Environ*. doi:[10.1007/s10064-015-0754-5](https://doi.org/10.1007/s10064-015-0754-5)
- Sui W, Liu J, Hu W, Qi J, Zhan K (2015) Experimental investigation on sealing efficiency of chemical grouting in rock fracture with flowing water. *Tunn Undergr Sp Tech* 50:239–249. doi:[10.1016/j.tust.2015.07.012](https://doi.org/10.1016/j.tust.2015.07.012)
- Takagi T, Sugeno M (1983) Derivation of fuzzy control rules from human operator's control actions. In: Proceedings of the IFAC symposium on fuzzy information, knowledge representation and decision analysis, pp 55–60
- Tekin E, Akbas SO (2011) Artificial neural networks approach for estimating the groutability of granular soils with cement-based grouts. *B Eng Geol Environ* 70(1):153–161. doi:[10.1007/s10064-010-0295-x](https://doi.org/10.1007/s10064-010-0295-x)
- Tinoco J, Correia AG, Cortez P (2011) Support vector machines in mechanical properties prediction of jet grouting columns. *Semana da Engenharia* 2011. <http://hdl.handle.net/1822/15084>
- Tinoco J, Correia AG, Cortez P (2012) Application of a sensitivity analysis procedure to interpret uniaxial compressive strength prediction of jet grouting laboratory formulations performed by SVM model. In: ISSMGE-TC 2i 1 international symposium on ground improvement Is-Gi, 317–326
- Tinoco J, Gomes Correia A, Cortez P (2014a) Support vector machines applied to uniaxial compressive strength prediction of jet grouting columns. *Comput Geotech* 55:132–140. doi:[10.1016/j.compgeo.2013.08.010](https://doi.org/10.1016/j.compgeo.2013.08.010)
- Tinoco J, Correia AG, Cortez P (2014b) A novel approach to predicting Young's modulus of jet grouting laboratory formulations over time using data mining techniques. *Eng Geol* 169:50–60. doi:[10.1016/j.enggeo.2013.11.015](https://doi.org/10.1016/j.enggeo.2013.11.015)
- Tran H, Hoang N (2014) An artificial intelligence approach for groutability estimation based on autotuning support vector machine. *J Constr Eng* 2014:1–9. doi:[10.1155/2014/109184](https://doi.org/10.1155/2014/109184)
- Uromeihy A, Barzegari G (2007) Evaluation and treatment of seepage problems at Chapar-Abad Dam, Iran. *Eng Geol* 91(2):219–228
- Utsuki S, Mito Y (2014) Experimental study of grouting for mechanical improvement of bedrock. In: ISRM international symposium-8th Asian rock mechanics symposium
- Wang S, Hao Z (2001) The genetic algorithm-neural network method to forecast the miniature crack grouting in rock matrix. *Chin J Geotech Eng* 23(05):572–575
- Xu HF, Wang C, Li CF, Jiang M, Geng HS, Chen F (2013) Estimating diffusion radius grouting into broken rock mass. *Appl Mech Mater* 353–356:44–49. doi:[10.4028/www.scientific.net/AMM.353-356.44](https://doi.org/10.4028/www.scientific.net/AMM.353-356.44)
- Yan F (2014) Theories and applications of unified grouting model and analysis in hydraulic and hydroelectric projects. Tianjin University, Tianjin (in Chinese)
- Yang C (2004) Estimating cement take and grout efficiency on foundation improvement for Li-Yu-Tan dam. *Eng Geol* 75(1):1–14. doi:[10.1016/j.enggeo.2004.04.005](https://doi.org/10.1016/j.enggeo.2004.04.005)
- Yang X, Li Y (2008) Construction and quality analysis of curtain grouting in foundation of dam for Yangtze Three Gorges project.

- Geotechnical engineering for disaster mitigation and rehabilitation. Springer, Berlin, pp 790–796
- Yang M, Chen M, He Y (2001) Current research state of grouting technology and its development direction in future. *Chin J Rock Mech Eng* 20(6):839–841
- Yang MJ, Yue ZQ, Lee PK, Su B, Tham LG (2002) Prediction of grout penetration in fractured rocks by numerical simulation. *Can Geotech J* 39(6):1384–1394. doi:[10.1139/t02-063](https://doi.org/10.1139/t02-063)
- Zadhesh J, Rastegar F, Sharifi F, Amini H, Nasirabad HM (2015) Consolidation grouting quality assessment using artificial neural network (ANN). *Indian Geotech J* 45(2):136–144. doi:[10.1007/s40098-014-0116-4](https://doi.org/10.1007/s40098-014-0116-4)
- Zettler AH, Poisel R, Reichl I, Stadler G (1997) Pressure sensitive grouting (PSG) using an artificial neural network combined with fuzzy logic. *Int J Rock Mech Min* 34(3):351–358
- Zhang L, Li Q, Song Y (2007) Neural network-based experimental study on shaft water sealing by grouting. In: Geoscience and remote sensing symposium, 2007. IGARSS 2007. IEEE International, pp 3142–3145
- Zhong DH, Yan FG, Li MC, Huang CX, Fan K, Tang JF (2015) A real-time analysis and feedback system for quality control of dam foundation grouting engineering. *Rock Mech Rock Eng* 48(5):1947–1968
- Zolfaghari A, Sohrabi Bidar A, Maleki Javan MR, Haftani M, Mehinrad A (2015) Evaluation of rock mass improvement due to cement grouting by Q-system at Bakhtiary dam site. *Int J Rock Mech Min* 74:38–44. doi:[10.1016/j.ijrmms.2014.12.004](https://doi.org/10.1016/j.ijrmms.2014.12.004)
- Ztürk CA, Nasuf E (2002) Geostatistical assessment of rock zones for tunneling. *Tunn Undergr Sp Tech* 17(3):275–285. doi:[10.1016/S0886-7798\(02\)00023-8](https://doi.org/10.1016/S0886-7798(02)00023-8)